Spring 2004

# Ultra-wideband technology for short-range wireless communication

Li Zhao
*New Jersey Institute of Technology*

## ABSTRACT

## ULTRA-WIDEBAND TECHNOLOGY FOR SHORT-RANGE WIRELESS COMMUNICATIONS

by
Li Zhao

The ultra-wideband (UWB) radio core idea is to open large amounts of spectrum to a variety of users with little mutual interference between them. While ultra-wideband is being championed by several commercial companies, this technology has not followed the conventional path where commercial interest is preceded by years of academic research. This work attempts to fill in some of the gap by studying fundamental properties of communications with impulse-based radio UWB signals. We study jam resistance and capacity of UWB. Jam resistance is analyzed for binary pulse position modulation (PPM) with the interference being modeled as correlated Gaussian. Closed-form expressions are provided for the jam resistance of a PPM UWB system utilizing rectangular pulses. Simple approximations are obtained for special cases (narrowband interference). Such analysis is extended to other practical UWB waveforms such as Gaussian and Rayleigh monocycles. It is shown that under some conditions, the UWB jam resistance is superior to that of direct sequence spread spectrum (DS-SS). In the second part of this work, we study the capacity of the single-user UWB communication systems utilizing M-ary PPM and bi-phase as well as on-off keying modulation scheme over additive white Gaussian noise (AWGN) and multipath channels. Starting from the known capacity of M-ary modulated signals, the computation of UWB capacity over the AWGN channel takes into account UWB specific constraints. The constraints are the power spectrum density limitation under Federal Communications Commission (FCC) Part 15 rules and the spreading ratio required to achieve a specified jam resistance level. UWB capacity over AWGN channel is expressed as a function of spreading ratio

and communication range. Trade-offs between capacity and range of communications and between capacity and spreading ratio are explored. We extend the study of capacity of UWB communications to the multipath channel using the modified S-V model proposed by the IEEE 802.15.3a task group. The complementary cumulative distribution function (CCDF) of the capacities, subject to the FCC power spectral density (PSD) limitation, are obtained for the all Rake (ARake) and selective Rake (SRake) receivers. In both of the cases, maximum ratio combining is employed. Finally, the capacity of multiple-access UWB communications is studied over the AWGN channel. Under certain assumptions, the multiple-access noise component at the receiver is modeled as Gaussian. An expression for the UWB capacity of the multiple-access channel is developed as a function of number of users.

# ULTRA-WIDEBAND TECHNOLOGY FOR SHORT-RANGE WIRELESS COMMUNICATIONS

by
Li Zhao

A Dissertation
Submitted to the Faculty of
New Jersey Institute of Technology
in Partial Fulfillment of the Requirements for the Degree of
Doctor of Philosophy in Electrical Engineering

Department of Electrical and Computer Engineering

May 2004

## APPROVAL PAGE

## ULTRA-WIDEBAND TECHNOLOGY FOR SHORT-RANGE WIRELESS COMMUNICATIONS

**Li Zhao**

Dr. Alexander M. Haimovich, Dissertation Advisor — Date
Professor, Department of Electrical and Computer Engineering, NJIT

Dr. Ali Abdi, Committee Member — Date
Assistant Professor, Department of Electrical and Computer Engineering, NJIT

Dr. Yeheskel Bar-Ness, Committee Member — Date
Professor, Department of Electrical and Computer Engineering, NJIT

Dr. Haim Grebel, Committee Member — Date
Professor, Department of Electrical and Computer Engineering, NJIT

Dr. Moe Win, Committee Member — Date
Assistant Professor, Department of Aeronautics and Astronautics, MIT

## BIOGRAPHICAL SKETCH

**Author:** Li Zhao

**Degree:** Doctor of Philosophy

**Date:** May 2004

**Undergraduate and Graduate Education:**

- Doctor of Philosophy in Electrical Engineering,
  New Jersey Institute of Technology, Newark, NJ, 2004
- Master of Science in Electrical Engineering,
  Nanjing University of Science Technology, Nanjing, P.R.China, 1997
- Bachelor of Science in Electrical Engineering,
  Nanjing University of Science Technology, Nanjing, P.R.China, 1994

**Major:** Electrical Engineering

**Presentations and Publications:**

L. Zhao, A.M. Haimovich and M.Z. Win, "Capacity of Ultra-Wideband Communications," *submitted to IEEE Transactions on Communications*, 2004.

L. Zhao and A.M. Haimovich, "Performance of Ultra-Wideband Communications in the Presence of Interference," *IEEE Journal on Selected Area in Communications*, vol. 20, No. 9, pp. 1684-1691, Dec., 2002.

L. Zhao, A.M. Haimovich and M.Z. Win, "Capacity of Ultra-Wide Bandwidth Communications over Multipath Channels," *2002 IEEE Symposium on Advances in Wireless Communications (ISWC '02)*, Sep. 23-24, 2002, Vancouver, BC, Canada.

L. Zhao and A.M. Haimovich, "Multi-user Capacity of M-ary PPM Ultra-Wideband Communications," *IEEE Conference on Ultra Wideband Systems and Technologies (UWBST)*, pp. 175-179, May 20-23, 2002, Baltimore, Maryland.

L. Zhao and A.M. Haimovich, "The Capacity of an UWB Multiple-Access Communications System," *IEEE InternationalConference on Communications (ICC '02)*, pp. 1964-1968, Apr. 28 - May. 2, 2002, New York City, New York.

L. Zhao and A.M. Haimovich, "Capacity of M-ary PPM Ultra-Wideband Communications over AWGN Channels," *IEEE Vehicle Technology Conference (VTC '01 Fall)*, pp. 1191-1195, Oct. 7-11, 2001, Atlantic City, New Jersey.

L. Zhao and A.M. Haimovich, "Interference Suppression in Ultra-Wideband Communications," *35th Annual Conference on Information Sciences and Systems (CISS '01)*, pp. 759-763, Mar. 21-23, 2001, The Johns Hopkins University, Baltimore, Maryland.

L. Zhao and A.M. Haimovich, "Performance of Ultra-Wideband Communications in the Presence of Interference," *IEEE International Conference on Communications (ICC '01)*, pp. 2948-2952, June. 11-15, 2001, Helsinki, Finland.

*To my dear husband Dongzhe and our lovely son Vincent*

## ACKNOWLEDGMENT

I am indebted to my thesis advisor Professor Alexander M. Haimovich, for introducing me to this research topic. I also acknowledge him for his constant help and encouragement through the years of my Ph.D study.

I would like to thank my dear husband and parents for their hard work and conditionless care and love that made this work possible.

## TABLE OF CONTENTS

## TABLE OF CONTENTS
## (Continued)

**Chapter** **Page**

## LIST OF FIGURES

## LIST OF FIGURES
## (Continued)

**Figure** **Page**

# CHAPTER 1

# INTRODUCTION

The expansion of information services in the last decade has affected the way we live and work. At present, the Internet continues to grow faster than any other global infrastructure in history. Parallel to the Internet, we have witnessed a phenomenal growth in wireless communications. Third generation (3G) wireless systems are designed to bring wireless data connections to mobile users. However, economical and architectural considerations as well as data rates limited to 2 Mb/s, severely limit the ability of 3G to provide tetherless Internet connections to densely packed users such as in hotels or airports.

Short-range wireless (SRW) is an alternative class of emerging technologies designed primarily for indoor use over very short distances [1]. SRW is intended to provide fast (tens or hundreds of megabits per second) and low cost, cableless connections to the Internet. SRW features transmission powers of several microwatts up to milliwatts yielding a communication range between 10 and 100 meter. SRW will provide connectivity to portable devices such as laptops, PDAs, cell phones, and others.

Short-range communications requirements lead to the emergence of a new category of networks referred to as personal area networks (PAN). PAN is designed for low power and low cost at the expense of range. New standards, such as Bluetooth and HomeRF, are being created to regulate short-range wireless communications. Ultra-wideband (UWB) is an emerging new technology that shows great potential for SRW applications.

UWB is almost two decades old, but used mainly in limited radar or position-location devices. Recent advancements in wireless communications generated

a renewed interest in UWB techniques. The fundamental principle of this technology is that a short pulse is generated, transmitted, received, and processed.

## 1.1 UWB Characteristics

The term "ultra-wideband" is referred to the spectral characteristics of this technology. Since the pulse width in UWB system is on the order of a nanosecond, according to the Fourier transform theory, such pulse occupies the frequency spectrum from near DC to a few gigahertz. UWB technology currently is defined by the Federal Communications Commissions (FCC) as any transmission scheme in which the fractional bandwidth $B_f$ is greater than 0.2 or the transmission bandwidth is more than 500MHz [2]. In the definition, the fractional bandwidth is determined as

$$B_f = \frac{2(f_H - f_L)}{f_H + f_L}, \tag{1.1}$$

where $f_L$ is the lower and $f_H$ is the higher -10 dB points in a spectrum, respectively.

The traditional impulse-based radio UWB technology has been developed over two decades when the original UWB signal definition was borrowed from the UWB Radar literature, where UWB is defined on the $B_f$. In the impulse-based radio UWB system, by transmitting the narrow pulses, the system uses all the frequency band simultaneously. Given the new definition in [2], UWB can apply to any technology that uses more than 500MHz spectrum. An alternative method emerging today uses a multiband approach in which information is encoded in multiple RF subbands at the same time, each occupying 500 MHz bandwidth.

In this dissertation, our research work is focusing on the traditional impulse-based radio UWB. In such system, the information data is encoded into the single pulse or pulse train by certain modulation scheme. The typical modulation well-suited for the impulse UWB is the pulse position modulation. For example, to convey the binary information, when the data symbol is "'1', a small time-shift is added to the

pulse train contained in a symbol duration, while there is no time shift when the data symbol is "0". Besides PPM, another two binary modulation scheme, bi-phase and on-off keying, are introduced as the alternatives for PPM in many UWB research literatures.

Time hopping is used in UWB as a multiple-access method. Multiple users can access the same bandwidth by each user having a distinct periodic pulse shift pattern. If the PPM scheme is employed in UWB system, these shift pattern generate an additional random-like time shift in addition to the PPM [3, 4].

The benefits of UWB technology are driven from its unique characteristics, these characteristics are:

- High data rate within the short range.

  From information theory, the large bandwidth is needed to transmit high data rate. The extreme wide bandwidth of UWB signals implies that such systems has great potential to provide high data rate. For example, our research work shows that for 1GHz channel bandwidth, UWB can achieve a data rate of 100 Mbits/s at a range of 20 m to 50 m, with a transmitted signal power of less than -41 dBm/MHz (FCC part 15 limit). This feature make UWB a promising technology for short-range wireless communications.

- High immunity to multipath.

  UWB short duration waveforms are relatively immune to multipath cancellation effects as observed in-building environments. Multipath cancellation occurs when a strong reflected wave - e.g., off of a wall, ceiling, vehicle, building, etc. - arrives partially totally out of phase with the direct path signal, causing a reduced amplitude response in the receiver. With very short pulses, the direct path has come and gone before the reflected path arrives and no cancellation occurs. It enable UWB signal well suited to operate in indoor environment with

applications like short-range wireless communications. In addition, multipath can be resolved easily by the UWB narrow pulses. Instead of discard those "echo" signals, by using the Rake receiver and the appropriate combining technique, the multipath component can be captured and added up together to enhance the signal-to-noise ratio at the receiver.

- Large processing gain and high covertness.

  UWB is a class of spread spectrum signal. It has a wide instantaneous bandwidth which is much larger than the bandwidth needed to transmit information [5]. In UWB system, the spread spectrum effect is generated directly by the extreme short pulses. It results in properties of the high covertness and large processing gain in UWB signals.

- Low cost, low power and small size.

  Most UWB device producers'goals are looking for the low cost, low power, small size design. This is also the trend of the whole wireless industry's bandwidth is inversely related to pulse duration, the spectral extent of these waveforms can be made quite large. With proper engineering design, the resultant energy densities (i.e., transmitted Watts of power per unit Hertz of bandwidth) can be quite low. Among the most important advantages of UWB technology, however, are those of low system complexity and low cost. UWB systems can be made nearly "all-digital", with minimal RF or microwave electronics. Despite of the inherent reason, low power and low cost can be achieved because the electronic can be completely integrated in CMOS without any inductive component. The antennas can be equally small and can be driven directly by CMOS.

High jam resistance, low power, immunity to multipath effects and overlay capability with other narrowband and wideband users make UWB very attractive for short-range applications.

## 1.2 UWB Regulation and Standardization

Since UWB sends the pulses across such a broad frequency range and because the pulse are so short (a nanosecond), it is very likely that UWB will cover the frequency-band of existing systems, such as wireless LAN's [6]. If the emissions from UWB devices are regulated to avoid causing significant interference to other services, then it becomes possible to allow UWB systems to operate on an unlicensed basis to enable UWB technology to support a diverse range of applications.

UWB is being promoted for non-licensed operation under Part 15 of the FCC Rules. This part commonly covers such consumer items as laptop, hair dryer, cordless phone, personal computers and garage door openers, that cannot conveniently be licensed. In order to minimize interference to licensed services, Part 15 devices are subject to significant constraints including the power and limitations and operations on a non-interference basis [7].

Since the 1990s, Federal Communications Commission (FCC) in US has been active in regulating UWB devices. In September 1998, the FCC initiated a Notice of Inquiry (NOI) to investigate the operation of ultra-wideband radio systems on an unlicensed basis under Part 15 rules. In May 2000, the FCC published a Notice of Proposed Rule Making (NPRM) on the revision of its Part 15 rules to include UWB systems. In its NPRM, the FCC tentatively proposed that UWB emission above approximately 2 GHz should comply with the normal Part 15 limits and that UWB emission below approximately 2 GHz be attenuated at least 12 dB below the Part 15 limits. After that, The FCC issued the requested three waivers for a limited number of each of three low power UWB devices, among them includes Time Domain's waiver for a limited number of life-saving, through-wall radar vision devices for use by the law enforcement and public safety communities.

Recently, The FCC Report and Order, issued in February 2002, allocated 7.5 GHz of the spectrum for the unlicensed use of UWB devices in the $3.1 - 10.6$ GHz

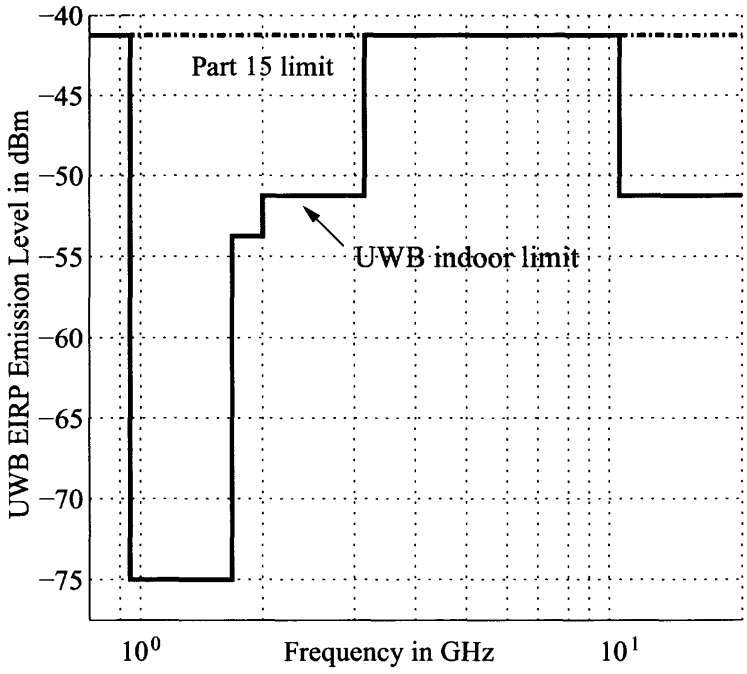


**Figure 1.1** UWB PSD mask for indoor applications.

frequency band [2]. UWB deployment in various applications was approved in [2] by limiting the average and peak emissions. The impact of UWB signals on a victim receiver appears to depend on the randomness of the UWB signal and the relationship between the pulse repetition frequency (PRF) of the UWB signals and the bandwidth of the receiver. If the pulse PRF is much larger than the bandwidth of the victim receiver, the emission of UWB signal may appear to be the random noise, the effect of UWB signal is proportional to the average power in UWB signal within the victim receiver's bandwidth. However, if the PRF is much less than the victim receiver's bandwidth, the UWB signal may appear to the receiver as impulse noise and the effect of UWB signal will be proportional to the peak power of the UWB signal. In order to reduce the potential for UWB emitters to cause the harmful interference under any circumstance, FCC conclude that it is necessary to regulate both the average and peak power emission levels [2].

The average power emission limit rules the power spectral density (PSD) measured in a 1 MHz bandwidth at the output of an isotropic transmitter antenna. Fig. 1.1 shows a mask representing the average PSD regulated by the FCC for indoor communications applications. The average PSD limit within the $3.1 - 10.6$GHz frequency band comply with the FCC Part 15 limit for unlicence device, which is $-41$dBm/MHz. Additional PSD limits have been placed below 2 GHz and above 10.6 to protect critical applications such as GPS. Also in [2], FCC regulates that UWB emissions have to comply with the peak emission limit of 0 dBm/50 MHz. FCC measurement shows the ratio of the peak-to-average power is proportional to $\mathrm{PRF}^{-1}$. When PRF $>$ 1 MHz, UWB emissions with the average emission limit $-41$ dBm/MHz also meet the peak emission limit 0 dBm/50 MHz. When PRF$<$ 1 MHz, the UWB transmissions at the average emission limit will exceed the peak emission limit [2]. Thus UWB emissions are average limited for PRFs greater than 1 MHz and peak-limited for PRFs below 1MHz.

Due to the unique characteristics of the UWB signals, the emerging UWB technology became an alternative potential solution for the IEEE 802.15 3a (TG3a) standard. The purpose of this standard is to provide a specification for a low complexity, low-cost, low-power consumption and high-date rate wireless connectivity for wireless personal-area network (WPAN). The date rate must be higher than 110 Mb/s to meet the demands for WPAN applications, such as personal digital assistants (PDAs), handheld personal computers (HPCs), as well as wireless home networking and so on. In addition, a new and complementary interest group to IEEE 802.15 3a was recently formed within IEEE 802.15.4 (IG4) to analyze the potential for a standard specifying a low-rate, low-power and low-cost WPAN technology based on UWB.

## 1.3 Overview of the Dissertation

The work presented in this dissertation is intended to study the fundamental aspects of UWB communications. The goal is to achieve a better understanding of the UWB performance in the presence of narrowband/wideband cochannel interference and of the theoretical bounds of UWB communications, as well as to develop techniques that will allow UWB to approach the communications bounds predicted by theory.

Chapter 2 introduces the general M-ary modulated UWB signal model. First, the various pulse waveforms utilizing in UWB system are described, and the temporal and spectral characteristics of those pulses are given. After that, the UWB signal model are obtained by defining various parameters used in this dissertation. The performance analysis in the following chapters is based on these pulse waveforms and signal model.

Chapter 3 describes the UWB channel model proposed by IEEE 802.15.3a task group. An UWB link budget is calculated based on the appropriate path loss model for UWB emissions. The performance of uncoded UWB system over the AWGN channel are studied.

Chapter 4 analyzes the performance of UWB communications in the presence of interference. The interference is modeled as a zero mean random process with constant power spectral density over a certain bandwidth. At the core of the UWB concept is the ability to cohabit the frequency spectrum with other signals. this means that both UWB communications will not be disturbed by cochannel interference and conversely, UWB signals will not be a source of interference to other applications in the same frequency range. While these requirements are well understood, not much analysis was published to flesh out the details. We refer to the ability to perform UWB communications in the presence of the interference as jam resistance. The implicit assumption has been that UWB has properties similar to conventional spread spectrum communications (such as direct sequence or frequency hopping),

namely that the jam resistance is proportional to the processing gain given by the ratio of signal bandwidth to information bandwidth. Hence the constraint on the duty cycle to meet a specified jam resistance. In our work, we found that the reality about jam resistance of UWB is more complex than previously assumed. In fact, we have shown that UWB PPM signals are significantly more jam resistant than direct sequence spread spectrum for narrowband interference (the likely practical case for UWB) [8, 9].

Chapter 5 computes the channel capacity of M-ary modulated single-user UWB communications. Two scenarios of the transmission channel are considered: AWGN channel and multipath channel. One of the main promises of UWB is to speed up wireless data transfer rates. Data rates of 40 Mbps to 8 Eps have been mentioned, but no analysis has been made available as to what is actually possible from a theoretical point of view. Our goal is to develop an understanding of the role of various parameters on the channel capacity of UWB communications. A literature search revealed work on PPM capacity done in the context of wireless infrared and optical channels [10, 11]. This work is applicable as a starting point for the analysis of the capacity of the UWB channel with PPM modulation. As the comparison, the capacity for the UWB system using bi-phase and on-off keying are also given in this chapter. The computation of UWB capacity for AWGN channel takes into account UWB specific constraints. The constraints are the power spectrum density limitation under FCC Part 15 rules and the spreading ratio required to achieve a specified jam resistance level. UWB capacity in AWGN channel is expressed as a function of spreading ratio and communication range. Also in this chapter, we extend the study of the UWB capacity into the multipath channel. The channel model used in this study is the modified Saleh-Valenzuela (S-V) model we described in Chapter 3. The performance analysis of the Rake receiver is conducted for an general L-tap Rake receiver when the maximum ratio combining (MRC) is employed. By

assuming the channel information is perfectly known at the receiver, the instantaneous capacity conditional on the channel information is developed for UWB system using M-ary modulation scheme. Due to the channel fading effect, such instantaneous capacities corresponding to the different channel realization are the random variables The complementary cumulative distribution function (CCDF) of the capacities are obtained for all Rake (ARake) receiver and selective Rake (SRake) receiver. Similar as the capacity over AWGN channel, outage capacity (such as 10% outage) of the UWB system over the multipath channel are illustrated as a function of spreading ratio and communication range subject to the FCC power spectral density (PSD) limitation. Due to the possible inter-symbol-interference (ISI) which occurs when the spreading ratio is too small, our study shows the trade off between the capacity and spreading ratio over the multipath channel are different from AWGN channel.

Chapter 6 studies the capacity for multiple-access UWB system over AWGN channel. Under certain assumptions, the multiple-access noise component at the receiver is modeled Gaussian. The capacity for multiple-access UWB system is derived from signal-to-noise ratio (SNR) considerations. A certain SNR is required to achieve a specified bit error probability (BEP). The noise floor raises with the number of users. Unlike the single-user capacity over AWGN channel in Chapter 5, capacity for multiple-access UWB system is developed as a function of the number of users. We assume UWB transmissions utilizing a rectangular pulse. It should be mentioned that the same analysis can be extended to other practical waveforms.

Chapter 7 summarizes the observations throughout this dissertation and suggest the future research for UWB communications.

# CHAPTER 2

# UWB SIGNAL MODEL

Impulse radio-based UWB is a fundamentally different information-transmission technique from today's modulated continuous-wave RF-carrier signals. The basic concept of UWB is to transmit and receive an extremely short duration burst of radio frequency (RF) energy - typically a few tens of picoseconds (trillionths of a second) to a few nanoseconds (billionths of a second) in duration. These bursts represent from one to only a few cycles of an RF pulse wave. The resultant waveforms are extremely broadband, so much so that it is often difficult to determine an actual RF center frequency - thus, UWB is called as "carrier-free" [12]. In such UWB system, the information data is encoded in the sequence of the UWB pulses in a variety of methods. The most popular modulation schemes developed to date for UWB are the pulse position modulation (PPM), on-off keying and the binary phase-shift keying (BPSK), also called bi-phase. In this chapter, first some basic pulse waveforms utilizing in the UWB system are introduced, then the UWB signal models using the different modulations mentioned above are proposed.

## 2.1 UWB Waveforms

The pulse waveform in UWB systems is constrained by FCC regulation 47 CFR Section 15.5(d), which states that "Intentional radiators that produce class B emissions (damped wave) are prohibited". Various non-damped waveforms have been proposed for impulse radio including Gaussian [4], Rayleigh, Laplacian and Cubic monocycles [13]. In general, the goal is to obtain a flat frequency spectrum of the transmitted signal over the bandwidth of the pulse and to avoid a DC component.

In this section, some basic pulse waveforms utilizing in the UWB system are introduced.

### 2.1.1 Rectangular Pulse

The rectangular pulse is not best suited for UWB applications, but is considered since it enables to obtain closed-form expressions when the performance analysis is studied. Such analysis is important since it provides insight into the mechanisms affecting the performance of UWB.

Let $p(t)$ be the UWB pulse waveform normalized to unit energy, $\int_{-\infty}^{+\infty} p(t)^2 dt = 1$. For a rectangular pulse $p_{re}(t)$ with pulse width $T_p$, we have

$$p_{re}(t) = \sqrt{\frac{1}{T_p}} \quad \text{if } 0 < t < T_p. \tag{2.1}$$

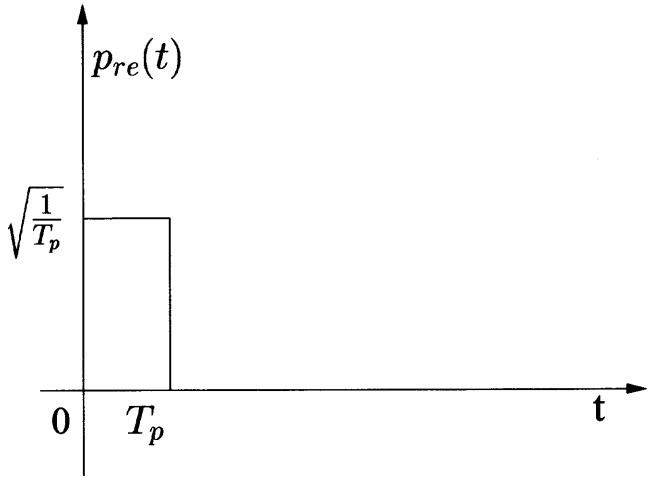


**Figure 2.1** Rectangular pulse.

The Fourier transform of $p_{re}(t)$ is a sinc function. The bandwidth of such time-limited rectangular pulse generally is regarded as $W = 1/T_p$. We have the time-bandwidth product $c$, which is defined as $c = WT_p$, is $c = 1$ for the rectangular pulse.

### 2.1.2 Monocycle Pulse

The practical waveforms utilizing in UWB system can be grouped in two category according the symmetrical characteristic in time. The Gaussian and Laplacian monocycle are even in time, while the Rayleigh and Cubic monocycle are odd. In this dissertation, we will focus on the study of the performance for a UWB communications system utilizing Gaussian and Rayleigh waveform. These two practical waveform have the complex mathematical formats and they are difficult to obtain a closed-form analysis, but the performance can still be studied by computer-aided numerical analysis.

Comparing with a rectangular waveform, the principal characteristic of the practical monocycle signals is that they have zero DC content to allow them to radiate effectively. The time domain representation of the Gaussian monocycle, $p_{ga}(t)$, is [13]:

$$p_{ga}(t) = A_{ga}\left(1 - \left(\frac{t}{\sigma}\right)^2\right)\exp\left(-\frac{t^2}{2\sigma^2}\right), \tag{2.2}$$

and a Rayleigh monocycle $p_{ra}(t)$ is given by

$$p_{ra}(t) = A_{ra}\left(\frac{t}{\sigma^2}\right)\exp\left(-\frac{t^2}{2\sigma^2}\right), \tag{2.3}$$

where $\sigma$ is a pulse width parameter. The amplitudes $A_{ga}$ and $A_{ra}$ are chosen such that each monocycle has unit energy. The time duration of the monocycle is $T_p = 7\sigma$. This interval contains 99.99 % of the total energy in the monocycle. Fig. 2.2 shows the monocycles with pulse width $T_p = 0.25$ ns.

The frequency spectrum of the Gaussian and Rayleigh monocycles are given by [13]:

$$S_{ga}(f) = A_{ga}\sqrt{2\pi\sigma^2}(2\pi\sigma f)^2\exp\left(-\frac{(2\pi\sigma f)^2}{2}\right), \tag{2.4}$$

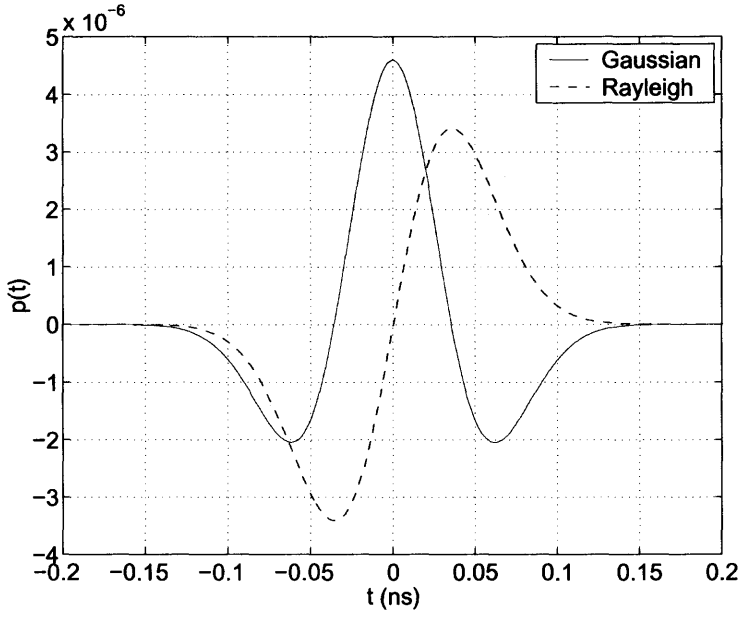


**Figure 2.2** UWB monocycles with $T_p = 0.25$ ns.

and

$$S_{ra}(f) = A_{ra}\sqrt{2\pi}(2\pi\sigma f)\exp\left(-\frac{(2\pi\sigma f)^2}{2}\right). \tag{2.5}$$

The effective bandwidth is defined as $W = f_H - f_L$, where $f_H$ and $f_L$ are the frequencies measured at the -10 dB emission points. Following the same numerical computation for -3 dB bandwidth in [13], our numerical evaluation shows that the Gaussian and Rayleigh monocycles have the $-10$ dB effective bandwidths:

$$W_{ga} = W_{ra} = 0.4301/\sigma. \tag{2.6}$$

Since pulse width $T_p = 7\sigma$, the bandwidth $W_{ga}$ and $W_{ra}$ are related to $T_p$ as following:

$$W_{ga} = W_{ra} = \frac{c}{T_p}, \tag{2.7}$$

where $c = 3.0110$. Fig. 2.3 is shown the frequency spectrums of the monocycles with $T_p = 0.25$ ns.

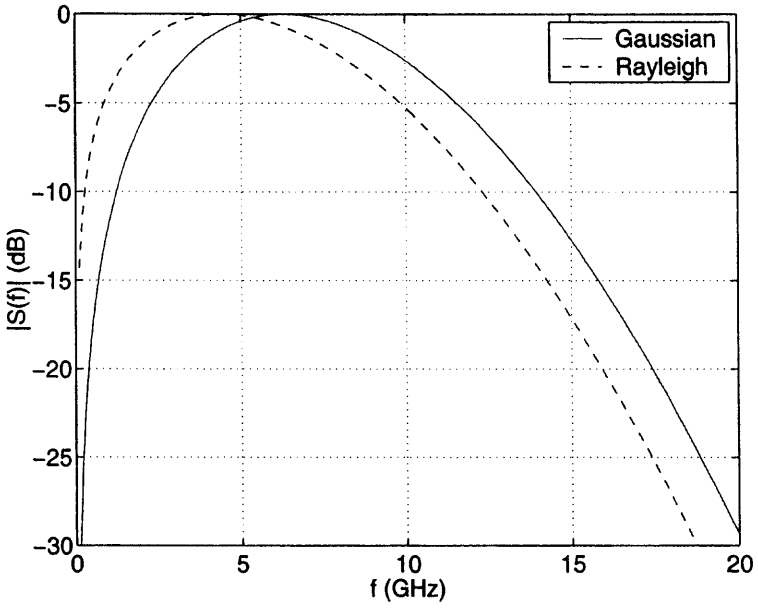


**Figure 2.3** Frequency spectrums of UWB monocycles.

## 2.2 UWB Signal Model and Assumptions

In this section, a signal model for the UWB communications system are proposed, in which the output of a k-bit source is encoded into M-ary signal wave form. This general signal model could be modified according to an M-ary PPM as well as the bi-phase and on-off keying signaling. Specially, for the PPM, only the orthogonal M-ary PPM signaling is studied, the overlapping PPM is not under consideration in this dissertation.

The sequence of UWB pulses for the $i$th symbol stream is referred to as $S_i(t)$, belonging to the M-ary signal set $(S_1(t), S_2(t), ..., S_M(t))$. $S_i(t)$ can be expressed

$$S_i(t) = \sum_{n=0}^{N_p-1} a_i \sqrt{E_p} p(t - b_i T_{PPM} - c_n T_c - nT_f), \quad 0 < t < N_p T_f, \quad i = 1, 2, ..., M \tag{2.8}$$

where, $p(t)$ is the UWB pulse of duration $T_p$ (normalized such that $\int_0^{T_f} p(t)^2 dt = 1$), the pulse waveform $p(t)$ can be modeled as rectangular pulse $p_{re}(t)$ or monocycles

$p_{ga}(t)$ and $p_{ra}(t)$. $E_p$ is the energy per pulses, and $T_f$ is the pulse repetition interval, referred to as *frame* interval. For a fixed $T_f$, the symbol rate $R_s = 1/(N_p T_f)$ determines $N_p$, the number of pulses that form a symbol. The symbol duration is then $T_s = N_p T_f$. $T_{PPM}$ is the time shift corresponding to the pulse position modulation. $c_n$ is the time hopping code assigned for active user during the $n^{th}$ frame. $a_i$ and $b_i$ are data sequence. Note that when $b_i = 0$, $S_i(t)$ is represented as a bi-phase signal if $a_i = \{-1, 1\}$ and an on-off keying if $a_i = \{0, 1\}$. Also $S_i(t)$ can be modified as an PPM signal given $a_i = 1$.

Based on the above general signal model, following assumptions are made in this dissertation:

1. For M-ary PPM, $T_{PPM} \geq T_p$ are assumed to obtain the orthogonal PPM signaling. We consider two kind of PPM scheme, one is $T_{PPM} = T_p$, and the other is $T_{PPM} = T_f/M$.

2. The parameter $N_p$ is the number of the UWB pulses transmitted for each data symbol, and it is related to UWB pulse repetition frequency (PRF) (defined as PRF=$1/T_f$) as PRF = $N_p R_s$. Obviously for certain symbol rate $R_s$, the UWB system with the lower PRF will encounter less inter-pulse-interference (IPI) over the practical channel (multipath channel). From this point of view, $N_p$ should be chosen as small as possible to get the low PRF UWB transmission and the ideal case for the minimum IPI is $N_p = 1$, which means the pulse repetition time $T_f = T_s$ and PRF = $R_s$ accordingly. However such ideal case is not allowable for $R_s < 1$ MHz by FCC regulations on UWB average and peak power limit. In [2], FCC measurement shows the ratio of the peak-to-average power is proportional to $\text{PRF}^{-1}$. When PRF > 1 MHz, UWB emissions with the average power $-41$ dBm/MHz (average emission limit) also meet the peak emission limit (lower than 0 dBm/50 MHz). When PRF< 1 MHz, the UWB transmissions at the average emission limit will exceed the peak emission limit

[2]. Thus for the UWB system with $R_s > 1$ MHz, $N_p$ could be chosen as 1 to get the minimum IPI over the multipath channel, at the meantime PRF is still high (PRF $= R_s > 1$ MHz) for UWB emission to meet both average and peak emission limit. For the other case, when $R_s < 1$ MHz, instead of $N_p = 1$, more pulses are transmitted in each symbol time. By doing this, PRF is increased to achieve the lower peak-to-average ratio, thus UWB signal emitted at average emission limit could meet the lowered peak power limit. For the purpose of less IPI, $N_p$ will be the minimum integer that meet PRF $= N_p R_s > 1$ MHz.

3. In the previous section, the time duration $T_p$ of UWB monocycle $p(t)$ is defined as interval contains 99.99 % of the total energy in the monocycle. Without loss of generality, we assume $p(t)$ exists only over the time interval $0 < t < T_p$. The effective bandwidth of pulse $p(t)$ is defined as $W = f_H - f_L$, where $f_H$ and $f_L$ are the frequencies measured at the -10 dB emission points. The bandwidth $W$ is related to pulse width $T_p$ as $W = c/T_p$, and $c \approx 3$ for Gaussian and Rayleigh monocycle. According to the FCC regulation, the effective bandwidth $W$ of the UWB signal should not exceed the range of $3.1 - 10.6$ GHz. In this dissertation, UWB system is considered operating in two possible frequency band as proposed recently in [14] to IEEE 802.15 3a group: low band from 3.1 GHz to 5.15 GHz or high band from 5.825 GHz to 10.6 GHz. Even though the dual-band mode (UWB signal can work in both of the two bands with duplexer) was also mentioned in [14], the dual-band mode will be not considered in study.

In [5], the effective bandwidth $W$ which was defined above is also called Fourier bandwidth. The notion of *Fourier bandwidth* will be used for $W$ instead of *effective bandwidth* in the remainder of the paper for the consistency with [5]. Also in [5], A Shannon bandwidth $B$ is defined as one half the minimum number of dimensions per second required to represent the modulated signal in a signal space. Simply speaking, the Shannon bandwidth is associated with symbol duration $T_s$ as $B = N/(2T_s)$, where

$N$ is the dimensionality of the signal. As examples, the M-ary PPM signal has the $N = M$ dimensionality, the Shannon bandwidth $B$ for the M-ary PPM signal then is $B = M/(2T_s)$. For the bi-phase and on-off keying signal, both of them has $N = 1$, therefore the Shannon bandwidth $B$ for these two signals is $B = 1/(2T_s)$.

In UWB system with symbol duration $T_s$, the value of the Shannon bandwidth $B$ can be interpreted as the minimum bandwidth required to transmit uncoded signal, and the Fourier bandwidth $W$ is the actual bandwidth *used* by UWB system. According to the definition in [5], UWB is spread spectrum in the sense that the UWB bandwidth $W \gg B$. The motivation for spread spectrum UWB is twofold: (1) attain specified level of transmitted power subject to power density constraints set by FCC Part 15 regulation, (2) attain specified level of resistance to other in-band emissions (jam resistance).

In [5], spreading ratio $\rho$ for the spread spectrum system is straightforwardly defined as the ratio of the Fourier bandwidth $W$ to the Shannon bandwidth $B$, e.g.:

$$\rho = \frac{W}{B}. \tag{2.9}$$

Since in our research, the Fourier bandwidth $W$ of UWB are given as either the low band ($W = 3.1-5.15$ GHz) or high band ($W = 5.825-10.6$ GHz.), it is of interest to develop the relationships between the spreading ratio $\rho$ with system parameters such as symbol rate $R_s$ and data rate $R_b$. From the definition of $R_s = 1/T_s$, $2T_sB = N$ and (2.9), we can obtain:

$$R_s = \frac{2W}{N\rho}. \tag{2.10}$$

The corresponding data rate can be expressed as

$$R_b = \frac{2W \log_2 M}{N\rho}. \tag{2.11}$$

The spreading ratio $\rho$ given in (2.9) are defined in the the frequency domain. Since two bandwidths in (2.9), $W$ and $B$, are related to two duration parameters in the time domain, $T_p$ and $T_s$ respectively, here we also define a parameter $\beta$ as

$$\beta = \frac{T_s}{T_p}. \tag{2.12}$$

So that $\beta$ can be viewed as an alternative of spreading ratio $\rho$ in the time domain. Even though $\beta$ is not equal to $\rho$ in quantity, both of them represent how much the spectrum is spread by using the narrow pulse waveforms in UWB system. $\beta$ is related to $\rho$ as

$$\beta = \frac{N}{2c}\rho. \tag{2.13}$$

As shown in (2.13), the only difference between the value of $\beta$ and $\rho$ is a factor determined by modulated signal dimensionality $N$ and time-bandwidth product $c$ of the UWB pulse waveform. In our following research, either $\beta$ or $\rho$ will be used depend on whether we perform the analysis in the time domain or in the frequency domain.

## 2.3 Chapter Summary

In first part of this chapter, some pulse waveforms utilizing in the UWB system, including the rectangular pulse and monocycles, are described. The temporal and spectral characteristics of these pulses are given. In the following chapters, the analysis of interference suppression and channel capacity are developed firstly for the UWB system utilizing the rectangular pulse, then extended to the UWB monocycles. From this study, the result shows that performance of UWB in the presence of interference are different for the UWB system utilizing the different pulse waveform. The future work is intended to develop the waveform design for anti-jammer, low probability of intercept, and high capacity.

At the second part, a general M-ary modulated UWB signal model is proposed. Various parameters in the signal model are defined. The performance analysis in the following chapters are based on this signal model.

# CHAPTER 3

# UWB CHANNEL MODEL

Numbers of UWB channel models have been proposed to IEEE 802.15.3a task group for the channel modeling as part of the physical layer (PHY) proposal in the future UWB communications standards. Most of the proposed models are based on the propagation measurements performed for indoor UWB channels. Among them, the stochastic tapped delay line (STDL) propagation model for UWB indoor channel given by [15] are frequently adopted by numerous UWB research papers. Another popular channel model proposed by Intel is a S-V model with a lognormal fading distribution on the channel responds amplitudes [16]. Recently, an modified S-V model was recommended for UWB communications by the channel modeling sub-committee of IEEE 802.15.3a task group. It is quit likely that this modified S-V model will be accepted in the future standards to evaluate the performance of UWB PHY layer. In this dissertation, we use this modified S-V model to conduct the UWB performance analysis over multipath channel.

## 3.1 Path Loss, Shadowing and Multipath Model

The path loss model PL is given by:

$$\mathrm{PL}(d, f) = 10 \log \frac{(4\pi)^2 d^n}{\lambda^2}, \tag{3.1}$$

where $n$ is the power attenuation exponent and $\lambda$ is the wavelength corresponding to the working frequency $f$. In an environment dense with obscuring objects, the received signal strength approximately follows $d^{-4}$-dependency with distance $d$. At short range such as several meters, the transmission is dominated by the direct signal path ($d^{-2}$ dependency). In the sub-committee final report about the UWB channel

modeling, IEEE P802.15 3a task group proposed to adopt the free space loss model ($n = 2$). People who use this model are allowed to justify parameters and estimate the required link margins for particular applications and deployment scenarios [17]. In our research, we calculate the UWB link budget based on the model given in (3.1) with $n = 2$.

Derived from the S-V model with some modifications, an UWB multipath channel model are proposed by IEEE P802.15 3a based on the observation of the clustering phenomenon as following [17]:

$$h(t) = \chi \sum_{p=1}^{P} \sum_{q=1}^{Q} h_{q,p} \delta(t - t_p - \tau_{q,p}), \tag{3.2}$$

where $h_{q,p}$ is the multipath gain coefficients. $t_p$ is the delay of the $p^{th}$ cluster, $\tau_{q,p}$ is the delay of the $q^{th}$ multipath component relative to the $p^{th}$ cluster arrive time $t_p$. $\chi$ represents the log-normal shadowing with the standard deviation $\sigma_\chi$. The distributions of $t_p$ and $\tau_{q,p}$ are depend on two parameters, cluster arrive rate $\Lambda$ and ray arrive rate $\lambda$, given by:

$$p(t_p|t_{p-1}) = \Lambda \exp\left[-\Lambda(t_p - t_{p-1})\right], \tag{3.3}$$

$$p(\tau_{q,p}|\tau_{q-1,p}) = \lambda \exp\left[-\lambda(\tau_{q,p} - \tau_{q-1,p})\right]. \tag{3.4}$$

The channel coefficients $h_{q,p}$ in the proposed model is $h_{q,p} = \alpha_{q,p}\beta_{q,p}$, where $\alpha_{q,p}$ is the equi-probable $\pm 1$ and $\beta_{q,p}$ is the log-normal random variable specified by $|\beta_{q,p}| \propto 10^{n/20}$. The parameter $n$ has the distribution $n \sim \mathcal{N}(\mu_{q,p}, \sigma_1^2 + \sigma_2^2)$, where $\sigma_1$ and $\sigma_2$ are the standard deviation of the cluster and the ray lognormal fading terms (dB) respectively. The $\mu_{q,p}$ is related to the model parameters as [17]

$$\mu_{q,p} = \frac{10\ln(\Omega_0) - 10t_p/\Gamma - 10\tau_{q,p}/\gamma}{\ln(10)} - \frac{\sigma_n^2 \ln(10)}{20}, \tag{3.5}$$

where $\Omega_0$ is the mean energy of the first path of the first cluster, $\Gamma$ and $\gamma$ are the cluster decay factor and the ray decay factor respectively.

Based on the practical channel measurement reported by the channel model contributions to IEEE 802.15 3a task group, the channel parameters in above models are determined to match the measured channel characteristics. In [17], four channel models for different channel scenarios (line-of-sight (LOS) or no-line-of-sight (NLOS), T-R separation within $0-4$m or $4-10$m) are provided. More detailed channel model adopted by IEEE 802.15 3a task group is available in [17].

By denoting $\tau_k = t_p - \tau_{q,p}$, above multipath channel model can be classified into the general tap-delay-line model given by:

$$h(t) = \chi \sum_{k=1}^{K} h_k \delta(t - \tau_k), \tag{3.6}$$

where $\tau_k$ is the delay of the $k$th multipath and $h_k$ is the correspondent multipath gain. $K$ is the total resolvable multipath number with $K = PQ$. The maximum delay spread of the multipath channel is $T_m$. Note that the realization of $h(t)$ in (3.6) is totally same as $h(t)$ in (3.2). In this paper, (3.6) was used instead of (3.2) in order to get the simpler expression in following analysis. In addition, the channel energy is assumed normalized to 1, e.g., $\sum_{k=1}^{K} h_k^2 = 1$ ($\sum_{p=1}^{P} \sum_{q=1}^{Q} h_{q,p}^2 = 1$).

## 3.2 UWB Link Budget

In February 2002, FCC published "First Order and Report" to permit and regulate UWB emissions for the certain type applications. In the report, UWB signals in the communication system should comply with the existing Part 15 limits and must operate in the frequency band of 3.1 GHz-10.6 GHz [2]. In this section, based on the path loss model recommended by IEEE 802.15.3a task group, the UWB link budget calculations is carried out assuming compliance with FCC Part 15 rules.

The commonly used link budget equation for narrowband emissions with center frequency $f$ is:

$$P_r(d, f) = P_t + G_t + G_r - \mathrm{PL}(d, f), \tag{3.7}$$

where $P_t$ is transmitted signal power; $P_r$ is received power at distance $d$; $G_t$ and $G_r$ are antenna gains for the transmitter and receiver respectively, both assumed 0 dB. The path loss PL is given in (3.1) with $n = 2$.

Since the received power in (3.7) is a function of frequency, and the bandwidth is too wide to ignore power variations across the band, we evaluate the UWB received power from

$$P_r^u(d) = \int_{f_L}^{f_H} \frac{P_r(d, f)}{W} df, \tag{3.8}$$

where $P_r(d, f)$ is the received power for a narrowband emission as in (3.7), in which average transmitted power $P_t$ is subjected to the FCC limitation on UWB transmission, e.g., $P_t \leq -41$ dBm/MHz. In (3.8), $f_H - f_L = W$, where $W$ is the UWB signal Fourier bandwidth. Substituting (3.7) and (3.1) into (3.8), we can obtain UWB received power $P_r^u(d)$ as

$$P_r^u(d) = P_t + G_t + G_r - 20 \log_{10} \left( \frac{4\pi d \sqrt{f_L f_H}}{c} \right). \tag{3.9}$$

In two band UWB system which we consider in this dissertation, $f_L = 3.1$ GHz and $f_H = 5.15$ GHz is for low band, while $f_L = 5.825$ GHz and $f_H = 10.6$ GHz is corresponding to the high band. From (3.9), it can be observed that the wider frequency bandwidth the UWB signal occupy, the more signal power loss it has due to the path loss.

To properly detect and decode the received signal, the receiver requires a certain minimum SNR. If we consider only thermal noise as the primary source of interference,

the received noise PSD $N_0$ can be calculated from:

$$N_0 = kTF, \tag{3.10}$$

definition where $k$ is the Boltzmann's constant $1.38 \times 10^{-23}$ Joules/K, $T$ is the room temperature (typically taken as 300 K), and $F$ is the noise figure (optimistically) assumed $F = 7$ dB. The noise power for a UWB receiver with bandwidth $W$ then can be calculated by $N_0W$. As a result, noise power for the low band UWB system is 80 dBm, and noise power $-77$ dBm can be obtained for the high band system

For the UWB system with the symbol energy $E_s$, the SNR per symbol (after demodulation SNR) is $\gamma_0 = 2E_s/N_0$, where $N_0/2$ is the two-sided noise power spectral density. Under the assumptions listed in Chapter 2, the average SNR at the input to the receiver is given by

$$\text{SNR}_{\text{in}} = \frac{P_r}{N_0W} = \frac{E_s/T_s}{N_0W}, \tag{3.11}$$

where $T_s$ is the symbol duration. Since we have the $2T_sB = N$ and $\rho = W/B$, for the UWB system with spreading ratio $\rho$, $\text{SNR}_{\text{in}}$ is related to $\gamma_0$ as following:

$$\text{SNR}_{\text{in}} = \frac{\gamma_0}{N\rho}. \tag{3.12}$$

A specified bit error probability performance determines the required SNR $\gamma_0$, which in turn sets the requirement for input SNR, $\text{SNR}_D$. The required sensitivity of the receiver is given by:

$$S = N_0W + \text{SNR}_D, \tag{3.13}$$

where all quantities are expressed in dBm or dB. In order to get the desired performance at a distance $d$, the received signal power should be equal or larger than the sensitivity, viz., $P_r^u(d) \geq S$. From (3.8) and (3.13), we can get relations between system parameters such as the spreading ratio $\rho$ and the maximum communications

range $d_{\max}$. For the M-ary modulated signal, the data rate $R_b$ is obtained by $R_b = \log_2 M/T_s$. Since we have the definition $T_s = N/(2B)$ and $B = W/\rho$, given the UWB bandwidth $W$, the transmitted data rate $R_b$ for M-ary modulated system can be expressed in terms of the spreading ratio $\rho$ as, $R_b = 2W\,(\log_2 M)\,/(N\rho)$. From this relation and (3.12), we have the following relation between the data rate and $\mathrm{SNR_{in}}$

$$R_b = \frac{2W\,(\log_2 M)}{\gamma_0}\mathrm{SNR_{in}}, \tag{3.14}$$

where $\gamma_0$ is the required SNR after demodulation for specified BEP performance over AWGN channel. Since $\mathrm{SNR_{in}}$ is function of distance $d$ and related to received power $P_r$ as shown in (3.11), data rate $R_b$ can also be expressed as a function of distance $d$.

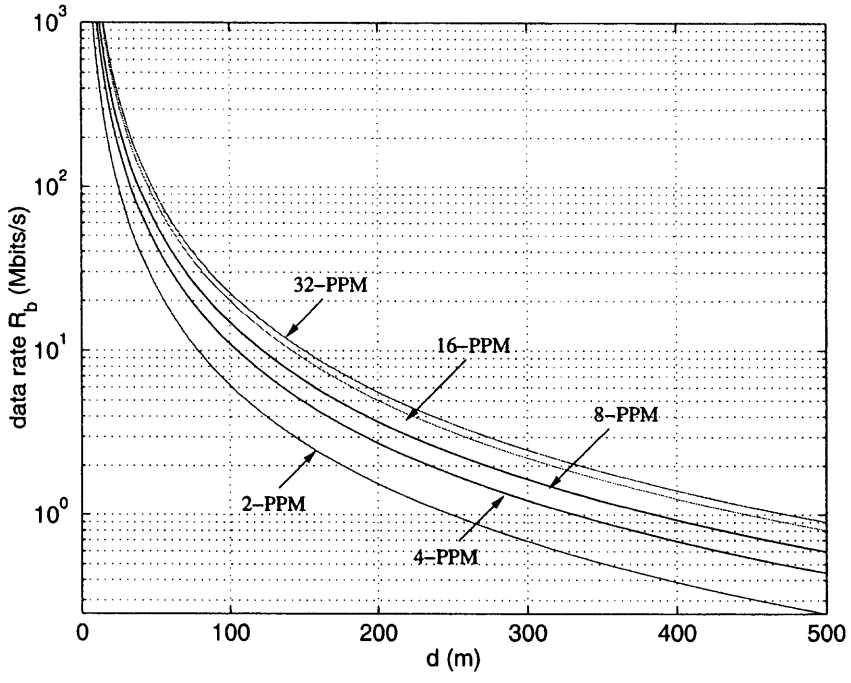


**Figure 3.1** Uncoded M-ary PPM UWB performance over AWGN channel at BER=$10^{-6}$ with $W = 3.1 - 5.15$ GHz.

Figure 3.1 and Fig. 3.2 demonstrate the trade-off between data rate and range for an uncoded M-ary PPM UWB communication system with the low band and high band respectively. The figures show the maximum range (subject to FCC Part 15 emission restrictions) at which the required signal to noise ratio $\gamma_0$ is still met as a

function of the data rate. The $\gamma_0$ requirement is computed for BEP $= 10^{-6}$. From Fig. 3.1 and Fig. 3.2, it can be observed that for the UWB uncoded system with the same modulation scheme, at the certain distance $d$, low band UWB system can achieve higher $R_b$ than the high band system. this result is due to the smaller path loss in low band UWB comparing with the high band UWB system.

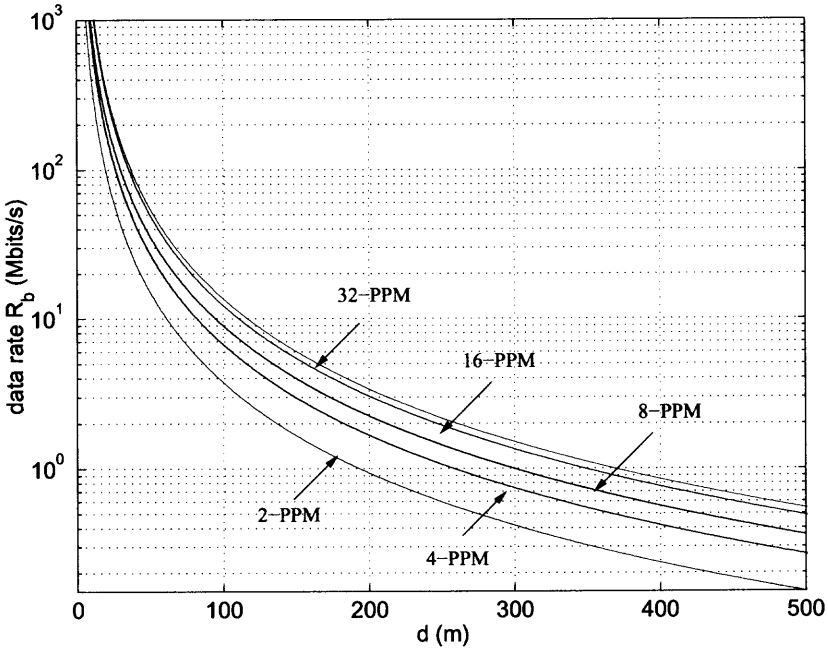


**Figure 3.2** Uncoded M-ary PPM UWB performance over AWGN channel at BER=$10^{-6}$ with $W = 5.875 - 10.6$ GHz.

## 3.3 Chapter Summary

In this chapter, a modified S-V model is described. This model is proposed by IEEE 802.15.3a task group and will be used in our following analysis. An UWB link budget is calculated based on the free space path loss model. As a result, an uncoded M-ary modulated UWB performance is studied over AWGN channel.

# CHAPTER 4

## INTERFERENCE SUPPRESSION IN UWB SYSTEM

Since gigahertz unoccupied slices of bandwidth are not available at microwave frequencies, under FCC regulations UWB radio must be treated as spurious interference to all other communication systems. In addition, UWB radios operating over the densely populated frequency range below a few gigahertz, must contend with a variety of interfering signals. These important requirements hint to similarities between UWB and the well-known spread spectrum technology. Like UWB systems, spread spectrum signals for digital communications have their beginnings in military communication due to: (1) their jam resistance capabilities and (2) low power spectral density, which makes them difficult to detect/intercept by an unintended listener. Recent results show that UWB signals have a lower detectability distance than certain commercial-off-the-shelf (COTS) spread spectrum systems with similar observation intervals, thus making UWB more covert than existing COTS systems [18].

Covertness is only one aspect of interest in comparing UWB to conventional constant-envelope spread spectrum modulations (such as direct sequence). Another characteristic of interest is the jam resistance capability. Jam resistance ability is measured by the processing gain defined in this context as the ratio of output and input signal-to-interference ratios. In this paper, we are concerned with analyzing jam resistance properties of UWB systems and comparing them to those of direct-sequence spread spectrum (DS-SS).

Processing gain of both UWB and DS-SS systems is obtained as a result of nonlinear filtering operations. With traditional DS-SS, the wide bandwidth is achieved by modulating the data message with a pseudo-noise (PN) sequence. The detected output signal-to-noise ratio is usually improved by the processing gain, which

is specified to be the ratio of the PN sequence chip duration to the information bit duration or equivalently, the processing gain is approximately the ratio of bandwidths of the spread spectrum and the information. This processing gain is obtained as a result of the PN property and the narrow chip of the modulating sequence. Unlike DS-SS, the spread bandwidth of the UWB waveform is generated directly and not by modulation with a separate spreading sequence. Thus, UWB is essentially a time-domain concept. The processing gain of UWB is due to the extremely short pulse, which generates a very wide instantaneous bandwidth signal, and is achieved at the receiver by time-gating matched to the pulse duration. Traditional DS-SS has a constant envelope with a 100% duty cycle and a peak power $P_{peak}$ equal to the average power $P_{av}$. With UWB, the pulse duration is extremely short with respect to the pulse repetition time resulting in pulse peak powers hundreds of time larger than the average power. To compare the performance of UWB and DS-SS, assume that they have the same average power $P_{av}$ (average power constraint), the same information sequence bit interval $T_b$ and that both are subject to an interference with average power $P_J$. Performance is assumed interference limited, hence the effect of additive white Gaussian noise is neglected. As the two systems have the same input signal-to-interference ratio (SIR), performance can be compared based only on the output SIR.

This chapter is organized as follows. Section 4.1 introduces the system model. The UWB performance analysis is developed in section 4.2. Comparison with DS-SS is carried out in section 4.3. Finally, conclusions and future works are provided in section 4.4 .

## 4.1 System Model

In this study of UWB interference suppression, a single-user UWB is considered. The general signal model for the single-user UWB is given in (2.8). To simplify the

theoretical analysis of jam resistance performance, we make the following additional assumptions:

1. No time-hopping code is used, i.e., $c_n = 0$.

2. To derive the performance of UWB in the presence of interference, we assume 2-PPM symbols. The pulse position time shift for data "1" equals the pulse width, i.e., $T_{PPM} = T_p$.

3. The parameter $N_p$ is the number of UWB pulses transmitted for each data symbol. For simplicity, and without loss of generality, we assume that for each data symbol, a single UWB pulse is transmitted ($N_p = 1$). This assumption implies the bit interval $T_b = T_f$. Since we consider the binary PPM, symbol time $T_s$ is equal to $T_b$, thus we have $T_s = T_f$ and $E_s = E_p$.

Based on above assumptions, the general UWB signal model given in (2.8) can be modified to the binary PPM signal of a single user $S(t)$. Therefore, over a bit interval $(n-1)T_b \leq t \leq nT_b, -\infty \leq n \leq \infty$, $S(t)$ can be written [4]:

$$S(t) = \sqrt{E_p} p(t - nT_f - \delta T_p). \tag{4.1}$$

The parameters $E_p$, $T_f$ and $T_p$ have the same definition as in (2.8). In addition, the parameter $\delta$ is the information binary sequence, e.g., $\delta = (0, 1)$.

Here the system performance is assumed interference limited. The effect of the thermal noise is neglected. The interference is represented by $J(t)$, then the signal at the receiver is

$$R(t) = S(t) + J(t). \tag{4.2}$$

The optimal receiver for a single user using UWB communications as defined so far, is a pulse correlation receiver. The template waveform used in the correlation

receiver is given by

$$V(t) = p(t) - p(t - T_p). \tag{4.3}$$

For a received signal $R(t)$, the correlation receiver computes

$$l_n = \int_{\tau+nT_f}^{\tau+(n+1)T_f} R(t)\, V(t - nT_f - \tau), \tag{4.4}$$

where $\tau$ represents the delay with respect to the time origin. Note that we assume perfect synchronization (known $\tau$). Decisions are made according to

$$d_n = \begin{cases} 1 & \text{if } l_n \geq 0 \\ 0 & \text{if } l_n \leq 0 \end{cases}. \tag{4.5}$$

The interference $J(t)$ is passband signal with carrier frequency $f_J$. It can be modeled as a continuous-time wide sense stationary, as illustrated in Fig. 4.1. It has zero mean value and constant power spectrum density $S_J(f)$ over the bandwidth $W_J$:

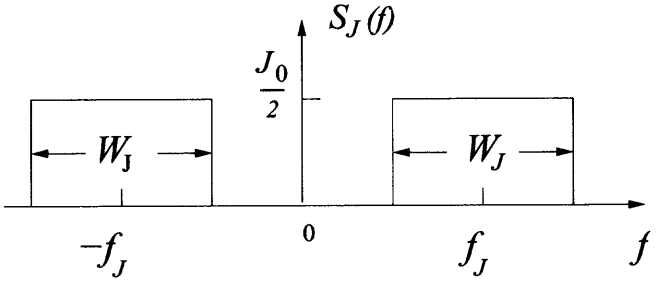


**Figure 4.1** Spectrum density of interference $J(t)$.

$$S_J(f) = \begin{cases} \frac{J_0}{2} & |f - f_J| \leq W_J \\ 0 & \text{otherwise} \end{cases}. \tag{4.6}$$

It follows that the autocorrelation $R_J(\tau)$ is:

$$R_J(\tau) = J_0 \frac{\sin \pi W_J \tau}{\pi \tau} \cos 2\pi f_J \tau. \tag{4.7}$$

With those assumptions, the signal received over a bit interval $(n-1)T_b \leq t \leq nT_b$, $-\infty \leq n \leq \infty$, is given by

$$R(t) = \sqrt{E_p}p(t - nT_f - \delta T_p) + J(t), \tag{4.8}$$

where $\delta \in \{0, 1\}$ is the information bit.

The cross-correlation $\int_0^{T_f} p(t - dT_p)v(t)dt$ over the pulse interval $T_f$ between the UWB pulse and the template at the receiver is 1 for $\delta = 0$ and $-1$ for $\delta = 1$. Hence, the correlator output corresponding to an information bit is given by:

$$\begin{aligned} y(nT_b) &= \int_{(n-1)T_b}^{nT_b} R(t)V(t - nT_f))dt \\ &= \pm\sqrt{E_p} + j(nT_b), \end{aligned} \tag{4.9}$$

where $\pm\sqrt{E_p}$ corresponds to the transmitted information bit '1' and '0', respectively, and $j(nT_b)$ represents the interference component.

Since $T_b = T_f$ (we assume $N_p = 1$), the interference component at the output of the correlator can be expressed by:

$$j(nT_b) = \int_{(n-1)T_f}^{nT_f} J(t)V(t - nT_f)dt. \tag{4.10}$$

The *processing gain* is defined as the ratio of the output to the input SIR,

$$\text{PG} = \frac{\text{SIR}_{\text{out}}}{\text{SIR}_{\text{in}}}. \tag{4.11}$$

The *Jam resistance* JR is defined as the margin that the processing gain provides above the minimum SIR, $\text{SIR}_D$ required to meet system performance specs:

$$\text{JR} = \text{PG} - \text{SIR}_D. \tag{4.12}$$

Let the power of a specified interference waveform $J(t)$ at the receiver input be $P_J$, and the signal power be $P_s$. The signal power can be expressed $P_s = E_b/T_b$ where

$E_b$ is the energy per information bit. Since $E_b = E_p$ (we assume $N_p = 1$), then the input SIR is given by

$$\text{SIR}_{\text{in}} = \frac{E_p}{T_b P_J}. \tag{4.13}$$

The SIR at the output of the UWB correlator receiver depends on the statistical characteristics of both the UWB signal and the interference:

$$\text{SIR}_{\text{out}} = \frac{E_p}{E[j^2(nT_b)]}. \tag{4.14}$$

From (4.11) and (4.13), (4.14), the processing gain is given by

$$\text{PG} = \frac{T_b P_J}{E[j^2(nT_b)]}. \tag{4.15}$$

The interference $J(t)$ is modeled by a random process, hence the functional $j(nT_b)$ is random variables. Assuming that the interference is wide-sense stationary, its power at the correlator output is expressed

$$\begin{aligned} E[j^2(nT_b)] &= E[\int_{(n-1)T_f}^{nT_f} J(t_1)V(t_1 - nT_f)dt \int_{(n-1)T_f}^{nT_f} J(t_2)V(t_2 - nT_f)dt_2] \\ &= \int_0^{T_f}\int_0^{T_f} R_J(t_1 - t_2)V(t_1)V(t_2)dt_1 dt_2. \end{aligned} \tag{4.16}$$

## 4.2 Performance Analysis

In this chapter, performance of UWB communications in presence of interference are explored for the systems utilizing the different pulse waveform. The analysis is first developed for UWB communications using rectangular pulse, then extended to the system with the monocycles.

### 4.2.1 Jam Resistance with Rectangular Pulse

The mathematic model of UWB rectangular pulse $p_{re}(t)$is given in (2.1). At the receiver, the corresponding template signal is

$$V_{re}(t) = \begin{cases} \sqrt{\frac{1}{T_p}} & \text{if } 0 < t < T_p \\ -\sqrt{\frac{1}{T_p}} & \text{if } T_p < t < 2T_p \end{cases} . \tag{4.17}$$

The waveform of $V_{re}(t)$ is shown in Fig. 4.2.

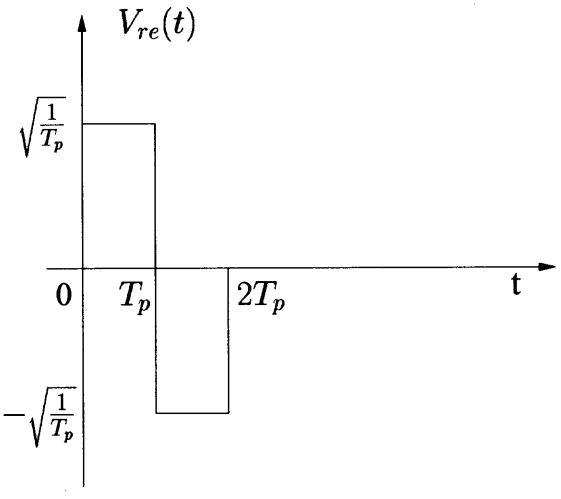


**Figure 4.2** Template signal $R_{re}(t)$.

Using (4.17) in (4.16), the time autocorrelation of the interference samples can be expressed [9]

$$\begin{aligned} E[j^2(nT_b)] &= \frac{1}{T_p}\int_0^{T_p}\int_0^{T_p} R_J(t_1 - t_2)dt_1dt_2 + \frac{1}{T_p}\int_{T_p}^{2T_p}\int_{T_p}^{2T_p} R_J(t_1 - t_2)dt_1dt_2 \\ &\quad -\frac{1}{T_p}\int_0^{T_p}\int_{T_p}^{2T_p} R_J(t_1 - t_2)dt_1dt_2 - \frac{1}{T_p}\int_{T_p}^{2T_p}\int_0^{T_p} R_J(t_1 - t_2)dt_1dt_2. \end{aligned}$$

Set $t_1 - t_2 = \tau$. Since the interference is assumed wide sense stationary, $R_J(\tau) = E[J(t)J(t-\tau)]$, $E[j^2(nT_b)]$ can be reduced to the single integral:

$$E[j^2(nT_b)] = \int_{-T_p}^{T_p}(1 - \frac{|\tau|}{T_p})[2R_J(\tau) - R_J(\tau + T_p) - R_J(\tau - T_p)]d\tau. \tag{4.18}$$

Substitute $R_J$ from (4.7) in (4.18), and set $\alpha = T_pW_J$, $x = W_J\tau$, $\beta = T_b/T_p$ and $\gamma = f_JT_p$. Note that $\alpha$ is the interference time-bandwidth product over the duration

of the pulse, $\gamma$ is number of cycles of the interference carrier frequency during an UWB pulse. Since we assume binary PPM and $N_p = 1$, from (2.13), $\beta = T_f/T_p$ is related to the UWB spreading ratio $\rho$ as $\beta = \rho/(2c)$ for the binary PPM (N=2), where $c$ is the time-bandwidth product of the UWB pulse waveform discussed in Chapter 2.

Then after some algebraic manipulations, (4.16) can be expressed:

$$E[j^2(kT_b)] = J_0\Phi(\alpha,\gamma), \tag{4.19}$$

where,

$$\Phi(\alpha,\gamma) = 2\Phi_0(\alpha,\gamma) - \Phi_1(\alpha,\gamma) - \Phi_2(\alpha,\gamma). \tag{4.20}$$

The quantities $\Phi_0(\alpha,\gamma)$, $\Phi_1(\alpha,\gamma)$, and $\Phi_2(\alpha,\gamma)$ are defined respectively,

$$\Phi_0(\alpha,\gamma) = \int_{-\alpha}^{\alpha}(1-\frac{|x|}{\alpha})\frac{\sin\pi x}{\pi x}\cos 2\pi\frac{\gamma}{\alpha}x dx, \tag{4.21}$$

$$\Phi_1(\alpha,\gamma) = \int_{-\alpha}^{\alpha}(1-\frac{|x|}{\alpha})\frac{\sin\pi(x+\alpha)}{\pi(x+\alpha)}\cos 2\pi\frac{\gamma}{\alpha}(x+\alpha)dx, \tag{4.22}$$

and

$$\Phi_2(\alpha,\gamma) = \int_{-\alpha}^{\alpha}(1-\frac{|x|}{\alpha})\frac{\sin\pi(x-\alpha)}{\pi(x-\alpha)}\cos 2\pi\frac{\gamma}{\alpha}(x-\alpha)dx. \tag{4.23}$$

From (4.14) and (4.16), the output SIR is then given by:

$$\mathrm{SIR_{out}} = \frac{E_p}{J_0\Phi(\alpha,\gamma)}. \tag{4.24}$$

Since, $E_p = E_b = P_sT_b$, $J_0 = P_J/W_J$, $T_bW_J = (T_pW_J)\,(T_b/T_p) = \alpha\beta$, we finally have

$$\mathrm{SIR_{out}} = \frac{P_s}{P_J}\frac{\alpha\beta}{\Phi(\alpha,\gamma)} = \mathrm{SIR_{in}}\frac{\alpha\beta}{\Phi(\alpha,\gamma)}. \tag{4.25}$$

The processing gain of UWB using a rectangular pulse is then given by

$$\mathrm{PG_{re}} = \frac{\alpha\beta}{\Phi(\alpha,\gamma)}. \tag{4.26}$$

Let us further discuss the physical meaning of the parameters $\alpha$, $\beta$ and $\gamma$ in (4.26).

1. The parameter $\alpha = W_J T_p$, serves as a measure of the ratio of bandwidths between the interference and the UWB waveform. Specifically, $\alpha \to \infty$ corresponds to an interference bandwidth much larger than that of the UWB signal, and $\alpha \to 0$ represents a narrowband interference. Due to filtering at the front-end of the receiver, the cases of interest are $0 \leq \alpha \leq 1$.

2. The variable $\beta = T_f/T_p$, is related to spreading ratio $\rho$ of a binary PPM UWB signals as $\beta = \rho/(2c)$. As we discussed in Chapter 2, the value of $c$ for the rectangular pulse is $c = 1$, while $c = 3$ is for the Gaussian and Rayleigh monocycles. Thus the processing gain of UWB with a rectangular pulse in (4.26) can be expressed as

$$\mathrm{PG_{re}} = \frac{\alpha\rho}{2\Phi(\alpha,\gamma)}. \tag{4.27}$$

3. The parameter $\gamma = f_J T_p$ measures the number of jammer carrier cycles during the UWB pulse. Since we consider only inband interference, $0 \leq \gamma \leq 1$.

When the interference is narrowband such that $\alpha \to 0$, we have the following approximations:

$$\Phi_0(\alpha \to 0, \gamma) = \int_{-\alpha}^{\alpha} (1 - \frac{|x|}{\alpha}) \cos 2\pi \frac{\gamma}{\alpha} x dx, \tag{4.28}$$

$$\Phi_1(\alpha \to 0, \gamma) = \int_{-\alpha}^{\alpha} (1 - \frac{|x|}{\alpha}) \cos 2\pi \frac{\gamma}{\alpha} (x+\alpha) dx, \tag{4.29}$$

$$\Phi_2(\alpha \to 0, \gamma) = \int_{-\alpha}^{\alpha} (1 - \frac{|x|}{\alpha}) \cos 2\pi \frac{\gamma}{\alpha} (x-\alpha) dx. \tag{4.30}$$

Combining these result in (5.23), we have $\Phi(\alpha \to 0, \gamma)$:

$$\Phi(\alpha \to 0, \gamma) = \frac{\alpha}{(\pi\gamma)^2}(1 - \cos 2\pi\gamma)^2. \tag{4.31}$$

From (4.27), when $\alpha \to 0$ the processing gain for a rectangular pulse is:

$$\mathrm{PG_{re}}(\alpha \to 0, \gamma) = \frac{\beta(\pi\gamma)^2}{(1 - \cos 2\pi\gamma)^2}. \tag{4.32}$$

To evaluate the jam resistance $\mathrm{JR_{re}}$ (defined in (4.12)) of an UWB system with a rectangular pulse, we assumed that the required system is a bit error probability of $P_b = 10^{-6}$. For 2-PPM, the corresponding $\mathrm{SIR}_D = 13$ dB, hence $\mathrm{JR_{re}} = \mathrm{PG_{re}} - 13$ (dB).

Fig. 4.5 illustrates the relationship between the jam resistance JR and parameter $\gamma$ for UWB with a rectangular pulse and $\beta = 100$ (corresponding spreading ratio $\rho = 200$). Of interest are cases of narrowband interference, $\alpha << 1$. The curves in the figure (except the one labeled $\alpha \to 0$) were generated using (4.26). The curve for $\alpha \to 0$ was generated using (4.32). It is observed that the jam resistance approaches its minimum value when $\gamma$ is in the neighborhood of 0.4 (corresponding to an interference carrier of $f_J = 0.4W$). Also shown in Fig. 4.5 is the case of wideband interference, $\alpha = 1$. The is approximately level at 7 dB (corresponding to $\mathrm{PG} - \mathrm{SNR}_D = 20 - 13$ dB).

### 4.2.2 Jam Resistance with Monocycles

Two different monocycles are chosen for analysis, Gaussian and Rayleigh. Temporal and spectral characteristics of the monocycles are shown in Fig. 2.2 and Fig. 2.3 respectively. For convenience, the subscript of all parameters use "mono" to represents these two monocycles instead of "ga" and "ra" for each of them. These two monocycles have pulse duration of $T_p = 1$ns and the bandwidth of $W = c/T_p$,

with $c = 3$. Received signals are correlated with the template waveform [8]:

$$V_{mono}(t) = p_{mono}(t) - p_{mono}(t - T_p). \tag{4.33}$$

Fig. 4.3 is shown the template waveforms for monocycles with $T_p = 1$ ns.

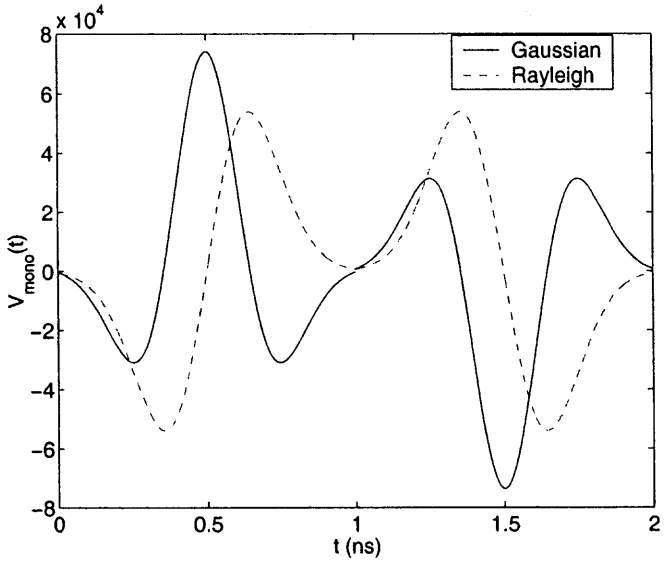


**Figure 4.3** Template signal for monocycles with $T_p = 1$ ns.

The goal is to evaluate the jam resistance (4.12), or equivalently, the processing gain (4.15). Using (4.7) in (4.16), we get

$$E[j^2(nT_b)] = \int_0^{T_f}\int_0^{T_f} J_0 \frac{\sin \pi W_J \tau}{\pi \tau} \cos 2\pi f_J \tau V_{mono}(t_1) V_{mono}(t_2) dt_1 dt_2. \tag{4.34}$$

Set $W_J t_1 = t_1'$, $W_J t_2 = t_2'$, and recall the definitions $\alpha = W_J T_p$, $\beta = T_f/T_p = \rho/(2c)$. and $\gamma = f_J T_p$. Then, $E[j^2(nT_b)]$ can be expressed

$$E[j^2(nT_b)] = J_0 \Theta(\alpha, \gamma), \tag{4.35}$$

where $\Theta(\alpha, \gamma)$ is given by the expression:

$$\Theta(\alpha, \gamma) = \int_0^{2\alpha}\int_0^{2\alpha} \frac{\sin \pi(t_1' - t_2')}{\pi(t_1' - t_2')} \cos 2\pi \frac{\gamma}{\alpha}(t_1' - t_2') V_{mono}(\frac{t_1'}{W_J}) V_{mono}(\frac{t_2'}{W_J}) dt_1' dt_2'. \tag{4.36}$$

Since by assumption $E[J(t)] = 0$, clearly the mean value of the interference component at the output of the receiver $E[j(nT_b)] = 0$. From (4.15) and (4.35), the processing gain for monocycles is given by

$$\mathrm{PG}_{\mathrm{mono}} = \frac{\alpha\beta}{\Theta(\alpha,\gamma)}, \tag{4.37}$$

where $\Theta(\alpha,\gamma)$ is computed for either the Gaussian or Rayleigh monocycles.

Comparing the processing gain of monocycles in (4.37) with that of the rectangular pulse in (4.26), we observe that they have the same format except for the different factors $\Theta$ and $\Phi$, which are determined by the specific pulse waveform.

Similar to the analysis for rectangular pulse, we chose the parameter $\beta = 100$ (corresponding spreading ratio $\rho = 600$) for computing the jam resistance of monocycles. In Fig. 4.6, jam resistance of three types of waveforms is plotted for an interference carrier with $0 < \gamma < 1$ and two values of the interference time-bandwidth product over the duration of the UWB pulse. Other than a small area when $\gamma > 0.8$, the suppression ability of the monocycles significantly exceeds that of the rectangular pulse. The Gaussian pulse provides the highest overall jam resistance. For all waveforms, the curves for $\alpha = 10^{-1}$ almost overlap with those for $\alpha = 10^{-3}$.

## 4.3 Comparison of UWB and DS-SS

Communications utilizing UWB and conventional direct sequence spread spectrum signals are similar in the sense that both use a short pulse (PN chip in DS-SS) to get the spread spectrum effect. But, there are fundamental differences between the two systems. The UWB waveform is at baseband and it does not have a constant envelope. Conversely, DS-SS signals have a constant envelope with the information waveform being modulated by a spread spectrum waveform and a carrier frequency. Furthermore, in typical applications, the chip of DS-SS will have a much longer duration than the UWB pulse width. Hence, the same interference with a

certain bandwidth $W_J$, could be narrowband with respect to UWB and wideband with respect to DS-SS. For UWB, the parameter $\alpha$ was defined as pulse width x interference bandwidth. This definition can be extended to DS-SS, where the pulse width is the chip time $T_c$. For DS-SS, $\alpha = T_c W_J$. Thus $\alpha$ serves as a measure of comparative bandwidth between the interference and either system. It is of interest to compare the performance of the two systems in the presence of interference. Notably, the mechanisms for interference suppression are quite different. With DS-SS, the interference is typically spread by cross-correlation with the PN sequence and is subsequently reduced by low-pass filtering at the data bandwidth. In contrast, with UWB there are two mechanisms for interference suppression: (1) time windowing over the duration of the short UWB pulse, (2) the cross correlation at the receiver of the interference with the template (4.3) results in reduction of a narrowband interference due to the high correlation of the interference at times $t$ and $t - \delta$.

### 4.3.1 Jam Resistance of DS-SS

To proceed with the comparison between UWB and DS-SS, consider a DS-SS system utilizing binary PSK, with a bit interval $T_b$, chip interval $T_c$, and spreading factor $L_c = T_b/T_c$. Within the bit interval $0 \leq t \leq T_b$, the transmitted signal is [19]:

$$S(t) = \sum_{n=0}^{L_c-1} d_0 \sqrt{\frac{2E_b}{T_b}} c_n p_c(t - nT_c) \cos 2\pi f_c t, \tag{4.38}$$

where $d_0 = \pm 1$ is the information symbol, $c_n$ denotes the PN code sequence, $p_c(t)$ is the chip waveform (normalized such that $\int_{-\infty}^{+\infty} p_c^2(t)dt = 1$), and $E_c$ is the energy per chip. The energy per bit of the DS-SS is $E_b = L_c E_c/2$. The code chip sequence is uncorrelated such that $E[c_n c_m] = E[c_n]\,E[c_m]$ for $n \neq m$.

For comparison with the UWB Gaussian monocycle, assume that the DS-SS chip waveform $p_c(t)$ is a normal Gaussian pulse as shown in Fig. 4.4 and given by

$$p_c(t) = A_c \exp\left[-\frac{t^2}{2\sigma^2}\right], \tag{4.39}$$

where $\sigma$ is a chip width parameter and $A_c$ denotes the amplitude of the chip waveform. The amplitude $A_c$ is such that

$$\int_{-\infty}^{\infty} p_c(t)^2 dt = 1. \tag{4.40}$$

The pulse width is chosen $T_c = 7\sigma$, ensuring that the time-limited pulse contains more than 99% of the energy of the Gaussian waveform defined in (4.40).

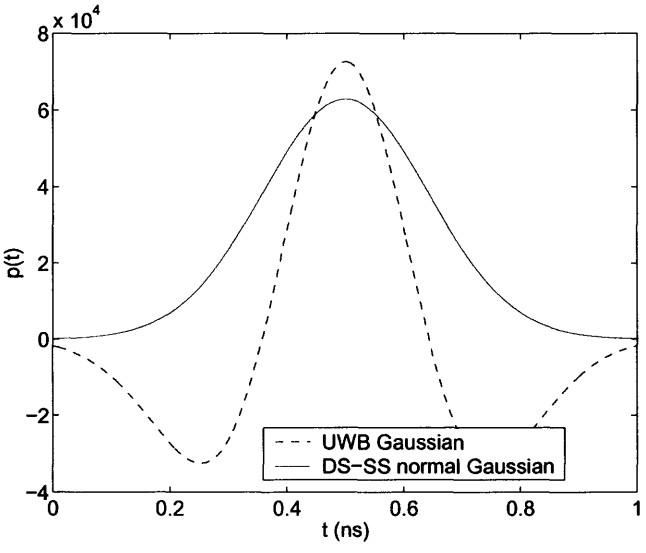


**Figure 4.4** Chip waveform of DS-SS.

The Gaussian monocycle is the derivative of the Gaussian pulse. In practice, the monocycle is the transmitted waveform resulting from high pass filtering by the transmit antenna of a Gaussian pulse. In Fig. 4.4 the temporal waveforms of normal Gaussian and Gaussian monocycle are compared with the same effective time duration.

Similar to the model in (4.8), the received signal $R(t)$ is corrupted by interference modeled by (4.6). Assuming ideal phase coherence and synchronization and the receiver, following carrier demodulation with $\cos 2\pi f_c t$ and despreading with the PN sequence $\sum_{n=0}^{L_c-1} c_n p_c(t-nT_c)$, the output of the DS-SS receiver at the sampling instant $t = T_b$ is:

$$y(T_b) = \pm\frac{1}{2}L_c\sqrt{E_c} + j(T_b), \tag{4.41}$$

where $j(T_b)$ represents the interference component, which has the form

$$j(T_b) = \int_0^{T_b} J(t) \sum_{n=0}^{L_c-1} c_n p_c(t - nT_c) \cos 2\pi f_c t \; dt = \sum_{n=0}^{L_c-1} c_n j_n, \tag{4.42}$$

where

$$j_n = \int_{nT_c}^{(n+1)T_c} J(t) p_c(t - nT_c) \cos 2\pi f_c t \; dt. \tag{4.43}$$

Since by assumption the PN sequence has uncorrelated terms,

$$E[j^2(T_b)] = L_c E\left[j_n^2\right]. \tag{4.44}$$

To evaluate the moment $E[j_n^2]$, we substitute $R_J(\tau)$ (4.7), into $E[j_n^2]$. By neglecting double frequency terms, we obtain the result

$$E\left[j_n^2\right] = \frac{J_0}{4}\int_0^{T_c}\int_0^{T_c} p_c(t_1)p_c(t_2)\frac{\sin \pi W_J(t_1 - t_2)}{\pi(t_1 - t_2)} \cos 2\pi(f_J - f_c)(t_1 - t_2)dt_1 dt_2. \tag{4.45}$$

Set $W_J t_1 = t_1'$, $W_J t_2 = t_2'$, $W_J T_c = \alpha$, and $\Delta f = f_J - f_c$. Then, $E[j_n^2]$ can be expressed as following:

$$E\left[j_n^2\right] = \frac{J_0}{4}\int_0^{\alpha}\int_0^{\alpha} p_c(\frac{t_1'}{W_J})p_c(\frac{t_2'}{W_J})\frac{\sin \pi(t_1' - t_2')}{\pi(t_1' - t_2')} \cos 2\pi\frac{\Delta f}{W_J}(t_1' - t_2')dt_1' dt_2'. \tag{4.46}$$

In (4.46), $\Delta f$ denotes the interference carrier offset with respect to the DS-SS carrier. If we define $\nu = \Delta f/W$, where $W$ is DS-SS bandwidth, $\nu$ measures the ratio of interference carrier to system bandwidth. Since there is assumed a passband prefilter

with bandwidth $W$ at the front end of the DS-SS receiver, for $-W/2 \leq \Delta f \leq W/2$, we have $-0.5 \leq \nu \leq 0.5$. Thus (4.46) can be written as:

$$E\left[j_n^2\right] = \frac{J_0}{4}\int_0^{\alpha}\int_0^{\alpha} p_c(\frac{t_1'}{W_J})p_c(\frac{t_2'}{W_J})\frac{\sin\pi(t_1'-t_2')}{\pi(t_1'-t_2')}\cos 2\pi\frac{\nu}{\alpha}(t_1'-t_2')dt_1'dt_2'. \tag{4.47}$$

Therefore the $\text{SNR}_{\text{out}}$ is:

$$\text{SNR}_{\text{out}} = \frac{E_b}{E[j^2(T_b)]} = \frac{E_b}{L_c\frac{J_0}{4}I(\alpha,\nu)}, \tag{4.48}$$

where $I(\alpha,\nu)$ is:

$$I(\alpha,\nu) = \int_0^{\alpha}\int_0^{\alpha} p_c(\frac{t_1'}{W_J})p_c(\frac{t_2'}{W_J})\frac{\sin\pi(t_1'-t_2')}{\pi(t_1'-t_2')}\cos 2\pi\frac{\nu}{\alpha}(t_1'-t_2')dt_1'dt_2'. \tag{4.49}$$

With the interference power spectral density $J_0 = P_J/W_J$ and the spread spectrum signal power $P_s = L_cE_c/2T_b$, we finally have

$$\text{SNR}_{\text{out}} = \frac{P_s}{P_J}\frac{2\alpha L_c}{I(\alpha,\nu)} = \text{SNR}_{\text{in}}\frac{2\alpha L_c}{I(\alpha,\nu)}. \tag{4.50}$$

It follows that the processing gain of DS-SS, $\text{PG}_{\text{DS-SS}}$ is:

$$\text{PG}_{\text{DS-SS}} = \frac{2\alpha L_c}{I(\alpha,\nu)}. \tag{4.51}$$

For a bit error probability the required SNR is $\text{SNR}_D = 10$ dB, hence the jam resistance of DS-SS is given by

$$\text{JR}_{\text{DS-SS}} = \frac{2\alpha L_c}{I(\alpha,\nu)} - 10(\text{dB}). \tag{4.52}$$

### 4.3.2 Comparison of Jam Resistance between UWB and DS-SS

Comparing the processing gain for UWB with a Gaussian monocycle (4.37) and DS-SS with Gaussian chips (4.51), it is observed that they have a similar form. Both processing gains are function of the parameter $\alpha$. As mentioned earlier, the parameter $\alpha$ measures the comparative bandwidth between the interference and either

system. Both parameters $\beta$ and $L_c$ have the same meaning of spreading factors which are the alternatives to the spreading ratio in the time domain. The two processing gain expressions contain different parameters for the interference carrier offset. With UWB, this parameter is $\gamma = f_J T_p$, while with DS-SS it is $\nu = (f_J - f_c)/W$. We can relate the two parameters as follows. Since UWB is carrier-less, we define the 'carrier' as the center frequency $W/2$ of UWB bandwidth. It follows that for UWB, the interference carrier offset is $\Delta f = f_J - W/2$. From the definition of $\gamma$, we have

$$\gamma = f_J T_p = \frac{\Delta f + W/2}{W} = \nu + \frac{1}{2}. \tag{4.53}$$

Figures 4.7 and 4.8 show the comparison of jam resistance with for $-0.5 \leq \nu \leq 0.5$, for wideband interference ($\alpha = 1$) and narrowband interference ($\alpha << 1$), respectively. The two figures were generated with the same bandwidth spreading factor for the both the UWB and DS-SS signals, i.e., $\beta = L_c = 100$. In Fig. 4.7, the wideband interference ($\alpha = 1$) has the same bandwidth as either system. It is observed that UWB has a higher jammer resistance than DS-SS over most of the range of $\nu$. Only when $\nu \to 0.5$, the curve of monocycle falls below that of DS-SS. As for narrowband interference shown in Fig. 4.8, it is obvious that the UWB system have a higher ability to suppress interference than DS-SS for most cases of $-0.5 \leq \nu \leq 0.5$. Furthermore, the advantage of UWB increases dramatically when $\nu \to -0.5$ and $\nu \to 0.5$. In another words, the jam resistance of UWB has a large variation as a function of the interference carrier frequency.

## 4.4 Chapter Summary

In this chapter, performance of UWB communications in the presence of interference was analyzed. Closed-form expressions were provided for the jammer resistance of a PPM UWB system utilizing rectangular pulses. Simple approximations were obtained for special cases (narrowband interference). Such analysis is extended to two practical

UWB waveforms: Gaussian and Rayleigh monocycles. A comparison between the interference suppression capabilities of UWB and DS-SS is executed under certain assumptions. It is shown that for wideband interference (interference bandwidth is equal to spread spectrum bandwidth) UWB has a advantage of interference suppression over DS-SS for most of case. The more practical situation is, however, a narrowband interference affecting the communication link. In this case, we showed that UWB has a better ability than DS-SS to suppress interference.

Above analysis about the jam resistance is just based on the system using binary PPM. Additional work is required to extend these results to multilevel PPM. Another issue that will be considered in the future work are signal processing for improved jam resistance and the effect on the jam resistance of the processing gain due to pseudorandom time hopping user code.

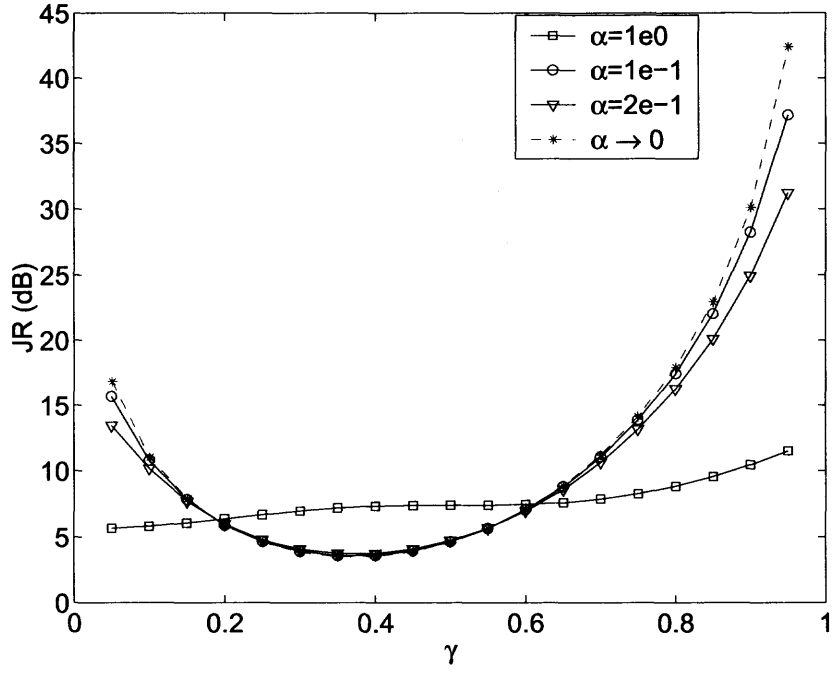


**Figure 4.5** Jam resistance of UWB utilizing rectangular pulse with different $\alpha$.

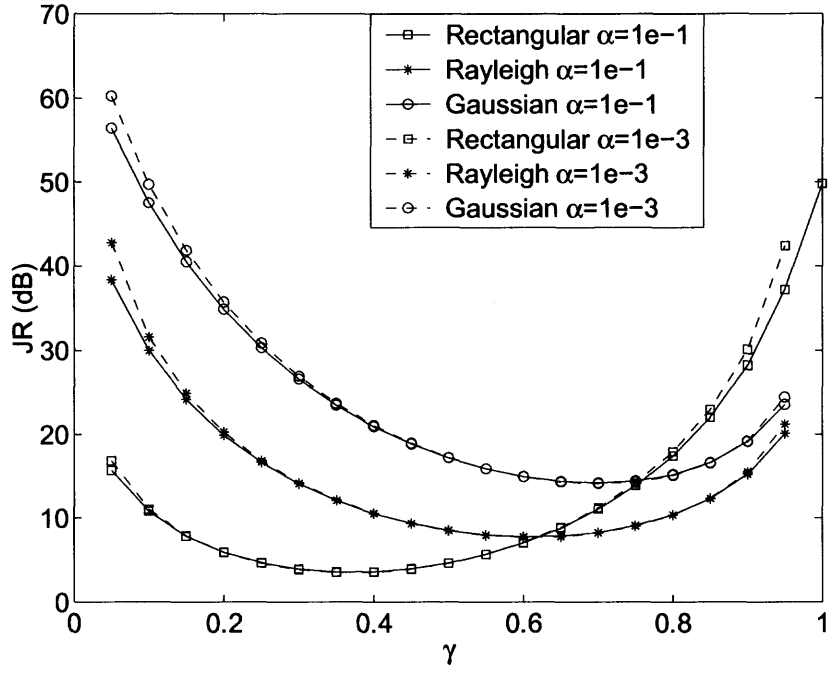


**Figure 4.6** Jam resistance of UWB utilizing monocycles with different $\alpha$.

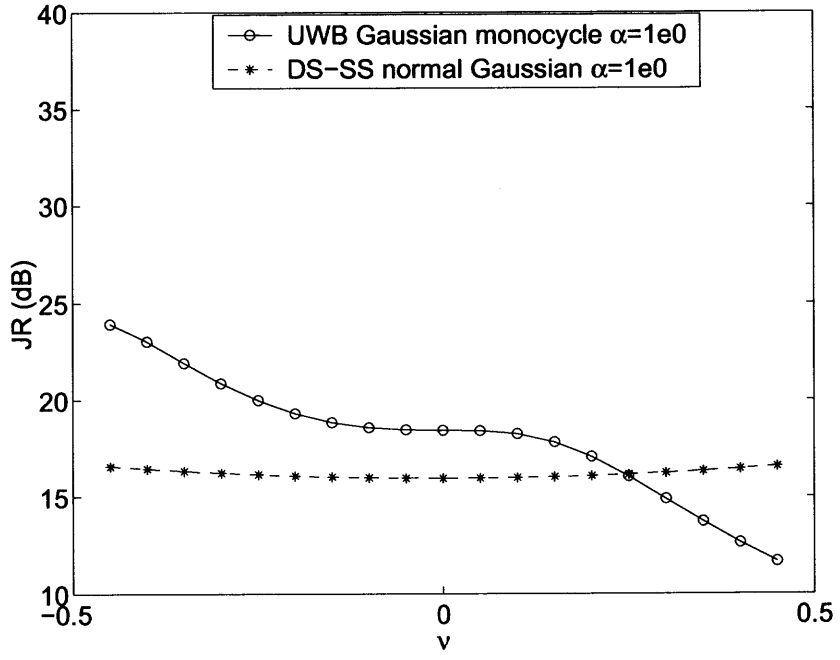


**Figure 4.7** Comparison between UWB and DS-SS on wideband interference suppression ($\alpha = 1$).

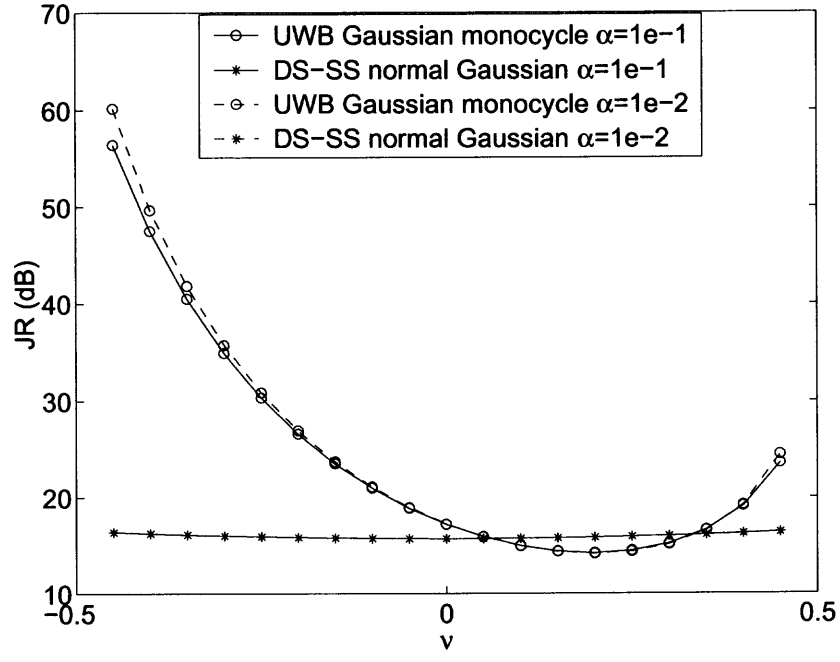


**Figure 4.8** Comparison between UWB and DS-SS on narrowband interference suppression ($\alpha << 1$).

# CHAPTER 5

# CAPACITY OF UWB SINGLE-USER SYSTEMS

UWB technology promises to deliver large amounts of data with very low power spectral density. The ultra-wideband radio concept is very attractive as it seeks to open large amounts of spectrum to a variety of users and at the same time it claims little interference between them. Unlike conventional wireless communications systems that are carrier-based, UWB-based communications is baseband. It uses a series of short pulses that spread the energy of the signal within a few GHz bandwidth.

From communication theory, with so extensive bandwidth occupied by UWB pulse, the UWB system has the potential to speedup wireless data transfer rates. Data rates of 40 Mbps to 2 Gbps have been mentioned, but little to no analysis has been made available as to what is actually possible from an information theoretic point of view.

In this chapter, the channel capacity of UWB communications system utilizing the different modulation schemes (PPM, bi-phase and on-off keying) was computed for the AWGN and multipath channels. The capacity of UWB is calculated with the UWB-specific constraints are added. These are the power spectrum density under FCC Part 15 rules and the spreading ratio constraints. Since gigahertz unoccupied slices of bandwidth are not available at microwave frequencies, under FCC regulations, UWB radio must be treated as spurious interference to all other communication systems. The FCC is currently allowing UWB emissions on an unlicensed basis for various applications. Unintended out of band emissions are governed by FCC Part 15 rules. In the study of UWB link budget in Chapter 3, it showed how the regulatory constraints on the PSD of the transmitted signal imposed by FCC affect the maximum range of UWB communication links. Thus it is of interest to study the information

theoretic channel capacity as a function of the distance between the transmitter and receiver.

A second UWB-specific constraint is the spreading ratio. The precise definition of spreading ratio for UWB has been given in Chapter 2. Here we can simply interpret the spreading ratio as the ratio between the bandwidth that UWB system *uses* and the bandwidth that UWB system *needs* to transmit the information. UWB is a spread spectrum method in the sense that it use more bandwidth than needed to carry the data. The spreading ratio is determined either from the requirement to 'hide' the UWB signal or conversely, from the requirement to suppress cochannel interference [20], which is also can be regarded as the requirement of the multiple access capability for the UWB multi-user system. Our goal is to develop an understanding of the role of spreading ratio play in determining the channel capacity of UWB communications.

Starting from the well known Shannon's capacity formula, we study the channel capacity for AWGN channel with continuous-valued inputs and outputs. This Shannon capacity expression is not the most suitable to communications with digital modulations. For instance, the capacity of communications channels utilizing PPM needs to take into account that PPM is a modulation with discrete-valued inputs and continuous-valued outputs and that PPM signals are orthogonal[10, 21]. we compute such discrete-valued inputs and continuous-valued outputs channel capacity for an PPM UWB system. As the comparison, capacities of UWB system with bi-phase and on-off keying are also discussed in this chapter.

Study of capacity for AWGN channel is important since it provide the insight into how fast and how far the UWB signal can carry the information over the ideal channel. However the practical UWB transmission channel is the multipath channel, especially for the indoor applications. Thus further study of capacity of UWB communications for the multipath channel becomes more interesting and attractive

for UWB system deployment in the real world, such as system configuration and UWB link coverage, etc.

Numbers of UWB channel models have been proposed to IEEE 802.15.3a task group for the channel modeling as part of the PHY proposal in the future UWB communications standards. In Chapter 3, we introduced the modified S-V model recommended by IEEE 802.15.3a task group. In this chapter, we will use this channel model to compute the UWB capacity.

The Rake receiver is employed to detect the signals in a multipath environment. In [22], an all Rake (ARake) receiver was defined as the receiver with the unlimited resources (taps or correlators)and instant adaptability, so that it can, in principle, combine all of the resolved multipath components. Alternatively, the selective Rake (SRake) receiver, which combines only the L strongest paths, may be employed. Here we study the capacity of multipath channel for these two types of Rake receivers. In both of the cases, maximum ratio combining is employed.

The reminder of this chapter is organized as follows. Section 5.1 gives the UWB signal model. Analysis of capacity for AWGN channel is carried out in Section 5.2, followed by the computation of capacity for multipath channel in Section 5.3. Finally, conclusions are provided in Section 5.4.

## 5.1 Single-User UWB Systems Model

The model for the single-user systems utilizing the M-ary modulation scheme can be obtained from the general UWB signal model given in (2.8). Since only one user are assumed operating in the system, we have $c_i^{(\nu)} = 0$. The transmitted signal $S_i(t)$, which is belonging to the M-ary signal set $(S_1(t), S_2(t), ..., S_M(t))$, can be expressed as

$$S_i(t) = \sum_{n=0}^{N_p-1} a_i \sqrt{E_p} p(t - b_i T_{PPM} - nT_f), \quad 0 < t < N_p T_f, \quad i = 1, 2, ..., M. \tag{5.1}$$

All the parameters in (5.1) have the same definitions as in (2.8). To calculate the UWB capacity, more assumptions are made on the signal model:

1. For the M-ary PPM, the time shift for the PPM $T_{PPM}$ are assumed as $T_f/M$.

2. The symbol energy $E_s$ is equal to $N_pE_p$, where $N_p$ is the number of the UWB pulses transmitted for each data symbol, and it is related to UWB pulse repetition frequency (PRF) (defined as PRF=$1/T_f$) as PRF $= N_pR_s$, where $R_s$ is the symbol rate. As we discussed previously in chapter 2, in order to meet both average and peak emission limit regulated by FCC, the value of $N_p$ is minimum integer that meet PRF $= N_pR_s > 1$ MHz.

Spreading ratio $\rho$ for UWB system is defined in (2.9). For every communication system, $\rho \geq 1$ and the equality holds only when ideal pulse waveform of sinc function are modulated [5]. For the UWB system with Fourier bandwidth $W = c/T_p$, we can obtain $\rho > 2c$ from (2.9) based on the previously assumption for PPM, which are $T_{PPM} > T_p$ and $T_s \geq T_f = MT_{PPM}$. Since the typical value of the $c$ for UWB pulses are around 3, we will consider the cases for $\rho \geq 5$ in this paper. When $\rho > 5$, UWB can be regarded as the spread spectrum system.

Communications utilizing UWB and DS-SS signals are similar in the sense that both techniques utilize short pulses (chips in DS-SS) to spread the spectrum. Yet, there are fundamental differences between the two methods. UWB is carrier-less and the pulses emitted by the transmitter are discontinuous. Conversely, DS-SS signals have a carrier and are time-continuous. With traditional DS-SS, the wide bandwidth is achieved by modulating the data message with a pseudo-noise (PN) sequence. The spectrum spreading is obtained as a result of the PN property and the narrow chip of the modulating sequence. Unlike DS-SS, the spread bandwidth of the UWB waveform is generated directly and not by modulation with a separate spreading sequence. The large spreading ratio of UWB is due to the extremely short pulse,

which generates a very wide instantaneous bandwidth signal, and is achieved at the receiver by time-gating matched to the pulse duration.

By its definition, spread spectrum is inefficient from the point of view of the spectral efficiency of a single user. As previously mentioned, its application in UWB is motivated by the need to keep the power spectral density low and to limit the effect of interference (which leads to the ability of multiple users to share the bandwidth).

Same as other spread spectrum systems, the larger spreading ratio will benefit an UWB system with the lower probability of interception, better electromagnetic compatibility and higher multiple-access capability. In the meantime, the large spreading ratio could reduce the bandwidth efficiency and results in the low capacity (bits/s) for UWB system. In the Section 5.2 and Section 5.3, we will examine the trade off between the UWB system capacity with the spreading ratio over AWGN and multipath channels.

## 5.2 Capacity of UWB Systems over AWGN Channel

In this section, the channel capacity for UWB single-user system will be computed. The channel model is assumed as the AWGN channel with two-sided noise spectral density $N_0/2$.

### 5.2.1 Shannon Capacity

For a communication system carrying the signal with Shannon bandwidth $B$ and the signal power as $P_r(d)$ at the T-R separation $d$ m, the Shannon capacity is given as [5]:

$$\mathcal{C}_{\text{Shannon}} = B \log_2 \left( 1 + \frac{P_r(d)}{N_0 B} \right) \quad \text{[bits/s]}. \tag{5.2}$$

From (5.2), it can be perceived that at T-R separation $d$ m, the higher capacity could be obtained either by increasing the signal power $P_r(d)$ or expanding the Shannon bandwidth $B$. We assume that the signal has been transmitted by its

maximum power, our following study will focus on the relation between the capacity and Shannon bandwidth $B$.

In the general communication system (non-spread spectrum system), the Shannon bandwidth $B$ is equal to the Fourier bandwidth $W$. Thus Shannon capacity for those non-spread spectrum system can be written as $\mathcal{C}_{\text{Shannon}} = W \log_2(1 + \frac{P_r(d)}{N_0 W})$. Since the Fourier bandwidth $W$ of communications system are always limited by the FCC, for the non-spread spectrum system, it is not practical to get the high capacity by expanding the Shannon bandwidth $B$.

Things are different for the spread spectrum system. Since $W >> B$, it is possible for system to achieve a higher capacity by increasing the bandwidth $B$ without requiring more Fourier bandwidth $W$. Obviously, to do so, spread spectrum system will lose the benefit of the spreading ratio which plays an important role in determining the jam resistance and multiple-access capability in spread spectrum system. Therefore, our UWB capacity analysis is carried out as a function of the spreading ratio.

Substituting (2.9) into (5.2), the Shannon capacity for spread spectrum UWB with bandwidth $W$ and spreading ratio $\rho$ can be written as:

$$\mathcal{C}^u_{\text{Shannon}} = \frac{W}{\rho} \log_2 \left(1 + \frac{P^u_r(d)}{N_0 W} \rho\right) \quad [\text{bits/s}]. \tag{5.3}$$

As we discussed in the previous section, the received UWB signal power $P^u_r(d)$ can obtained from $P^u_r(d) = P_t PL(d)^{-1}$, and $p(t)$ is limited by FCC part 15 rules. Thus at the T-R separation $d$ m, the capacity can be evaluated as:

$$\mathcal{C}^u_{\text{Shannon}} = \frac{W}{\rho} \log_2 \left(1 + \frac{P_t PL(d)^{-1}}{N_0 W} \rho\right) \quad [\text{bits/s}], \tag{5.4}$$

where $PL(d)$) is the UWB signal path loss model given in (3.1).

The trade off between the Shannon capacity $\mathcal{C}^u_{\text{Shannon}}$ with the spreading ratio $\rho$ is shown in Fig. 5.3 - Fig. 5.6. Among them, Fig. 5.3 and Fig. 5.4 are plotted for

the UWB system operating in the low band (3.1 GHz - 5.15 GHz), and Fig. 5.5 and Fig. 5.6 are generated for UWB system of the high frequency band (5.875 GHz - 10.6 GHz). For both of systems, $\mathcal{C}^{u}_{\text{Shannon}}$ is demonstrated by two manner. First we show $\mathcal{C}^{u}_{\text{Shannon}}$ as the function of T-R separation $d$ when the spreading ratio from $\rho = 5$ to $\rho = 500$ are prescribed. Then the capacity $\mathcal{C}^{u}_{\text{Shannon}}$ is illustrated as the function of $\rho$ for different case of $d$.

### 5.2.2 Discrete-Input Continuous-Output Capacity

In this section, we will compute the capacity for UWB system in AWGN channel when the digital modulation is considered.

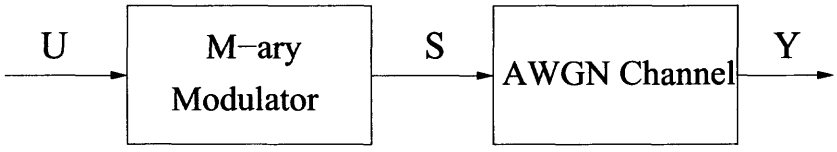


**Figure 5.1** M-ary modulated signal channel model.

For the discrete-valued input and continuous-valued output channel shown in Fig. 5.1, a $k$-bit information source $\mathbf{U} = (U_1, U_2, U_3, \ldots, U_k)$ is mapped to a $M = 2^k$ modulated signal set $\mathbf{S} = (S_1, S_2, \ldots, S_M)$. Specially for orthogonal M-ary PPM, signal $S_i$ can be represented as an $M$-dimensional vector $\mathbf{s}_i$. The PPM signal constellation of $\mathbf{S}$ is interpreted as a collection of points in $M$-dimensional signal space with one point located on each coordinate axis at a distance of $\sqrt{E_s}$ from the origin. The vector representation of $S_i$ for M-ary PPM is given by $\mathbf{s}_i = (0, \ldots, 0, \sqrt{E_s}, 0, \ldots, 0)$. For the one dimensional binary signal, such as bi-phase and on-off keying, $S_i$ can also be represented by the one dimensional vectors, e.g., $\mathbf{s}_1 = \sqrt{E_s}$ and $\mathbf{s}_2 = -\sqrt{E_s}$ for bi-phase signal, $\mathbf{s}_1 = \sqrt{E_s}$ and $\mathbf{s}_2 = 0$ for on-off keying signal. Capacity is the maximum amount of information that can be transmitted reliably and is given by $C = \max_{p(\mathbf{U})} I(\mathbf{Y}; \mathbf{U})$, where $I(\mathbf{Y}; \mathbf{U})$ is the mutual information between the channel output $\mathbf{Y} = (y_1, y_2, \ldots, y_M)$ and the channel

input $\mathbf{U}$, $p(\mathbf{U})$ is the M-ary source probability distribution. Since $\mathbf{S}$ is an invertible function of $\mathbf{U}$, the capacity can be expressed $C = \max_{p(\mathbf{S})} I(\mathbf{Y};\mathbf{S})$. In addition, as we consider the symmetrical M-ary modulated signals, capacity is achieved with a uniform source distribution, $p(\mathbf{S} = \mathbf{s}_i) = 1/M$, for $i = 1,..,M$. The capacity expression with respect to the symmetrical inputs $\{\mathbf{s}_1, ..., \mathbf{s}_M\}$ can be obtained

$$C_{\text{M-ary}}(\mathbf{Y};\mathbf{S}) = \int_{\mathbf{Y}} p(\mathbf{Y} \mid \mathbf{s}_1\}) \log_2 \left( \frac{p(\mathbf{Y} \mid \mathbf{s}_1\})}{\frac{1}{M}\sum_{i=1}^{M} p(\mathbf{Y} \mid \mathbf{s}_i\})} \right) d\mathbf{Y} \quad \text{[bits/symbol]}. \tag{5.5}$$

In M-ary PPM system, when the signal $\mathbf{s}_i$ is transmitted over the AWGN channel with two-sided noise spectral density $N_0/2$, the component of channel output $\mathbf{Y}$, are conditional independent Gaussian random variables

$$\begin{aligned} y_j \quad &\text{is} \quad \mathcal{N}(\sqrt{E_s}, N_0/2) \quad j = i \\ y_j \quad &\text{is} \quad \mathcal{N}(0, N_0/2) \quad\quad j \neq i, \end{aligned} \tag{5.6}$$

where the symbol $\mathcal{N}(a,b)$ denotes the Gaussian distribution with mean $a$ and variance $b$.

Therefore, the M-ary PPM capacity $C_{\text{M-PPM}}$ in AWGN channel as a function of the channel symbol SNR $\gamma_0 = 2E_s/N_0$ can be obtained by using the distribution of $y_j$ (in (5.6)) into (5.5), the final expression is given as in [10]

$$C_{\text{M-PPM}}(\gamma_0) = \log_2 M - E_{\mathbf{v}|\mathbf{s}_1} \log_2 \sum_{i=1}^{M} \exp\left[\sqrt{\gamma_0}(v_i - v_1)\right] \quad \text{[bits/symbol]}, \tag{5.7}$$

where the random variables $v_i$, $i = 1,..,M$ have the following distribution conditional on the transmitted signal $\mathbf{s}_1$ (due to the symmetry of M-ary PPM, any signal can serve to condition the output):

$$\begin{aligned} v_1 \quad &\text{is} \quad \mathcal{N}(\sqrt{\gamma_0}, 1) \\ v_i \quad &\text{is} \quad \mathcal{N}(0, 1) \quad i \neq 1. \end{aligned} \tag{5.8}$$

Even through M-ary PPM capacity has to be obtained by Monte Carlo runs of (5.7), it is possible to develop a closed form express for the special case of $M = 2$ as given in [23].

From (5.7), the capacity for binary PPM is given by

$$\begin{aligned} C_{\text{2-PPM}}(\gamma_0) &= 1 - E_{\mathbf{v}|\mathbf{X}_1} \log_2 \left(1 + \exp\left(\sqrt{\gamma_0}(v_2 - v_1)\right)\right) \\ &= E_{\mathbf{v}|\mathbf{X}_1} \log_2 \frac{2}{1 + \exp\left(\sqrt{\gamma_0}(v_2 - v_1)\right)} \quad \text{[bits/symbol]}. \end{aligned} \tag{5.9}$$

Computing the expected value using the Gaussian distributions of $v_1$ and $v_2$, we have:

$$\begin{aligned} C_{\text{2-PPM}}(\gamma_0) &= \frac{1}{2\pi} \int_{-\infty}^{+\infty} \int_{-\infty}^{+\infty} \exp\left(-\frac{(v_1 - \sqrt{\gamma_0})^2}{2}\right) \exp\left(-\frac{{v_2}^2}{2}\right) \\ &\quad \cdot \log_2 \frac{2}{1 + \exp\left(\sqrt{\gamma_0}(v_2 - v_1)\right)} dv_1 dv_2 \quad \text{[bits/symbol]}. \end{aligned} \tag{5.10}$$

Set $x = v_2 - v_1$, we finally obtain the capacity of binary PPM,

$$\begin{aligned} C_{\text{2-PPM}}(\gamma_0) &= \frac{1}{2\sqrt{\pi}} \int_{-\infty}^{+\infty} \exp\left(-\frac{(x - \sqrt{\gamma_0})^2}{4}\right) \log_2 \left(\frac{2}{1 + \exp\left(-\sqrt{\gamma_0}x\right)}\right) dx \\ &\quad \text{[bits/symbol]}. \end{aligned} \tag{5.11}$$

From communication theory, the capacity for on-off keying signal $C_{\text{on-off}}(\gamma_0)$ is same as the binary PPM capacity $C_{\text{2-PPM}}(\gamma_0)$ in (5.11), even though the dimensionality of two signals are different. Similarly, the capacity for bi-phase signaling can be obtained as:

$$\begin{aligned} C_{\text{bi-phase}}(\gamma_0) &= \frac{1}{\sqrt{2\pi}} \int_{-\infty}^{+\infty} \exp\left(-\frac{(x - \sqrt{\gamma_0})^2}{2}\right) \log_2 \left(\frac{2}{1 + \exp\left(-2\sqrt{\gamma_0}x\right)}\right) dx \\ &\quad \text{[bits/symbol]}, \end{aligned} \tag{5.12}$$

due to the component of channel output $\mathbf{Y}$ for the bi-phase signaling is

$$\begin{aligned} y_j \quad &\text{is} \quad \mathcal{N}(\sqrt{E_s}, N_0/2) \qquad j = i, \ (i, j = 1, 2) \\ y_j \quad &\text{is} \quad \mathcal{N}(-\sqrt{E_s}, N_0/2) \qquad j \neq i, \ (i, j = 1, 2). \end{aligned} \tag{5.13}$$

The capacities in (5.7), (5.11) and (5.12) are alone evaluated as function of the channel symbol SNR $\gamma_0$. To make them applicable to UWB, it is necessary to customize the expression of $\gamma_0$ for UWB. Next the specific UWB constraints will be added.

As we mentioned before, Shannon bandwidth $B$ for an modulated signal is related to symbol time $T_s$ as $B = N/(2T_s)$. Thus in the UWB system with Fourier bandwidth $W$ and spreading ratio $\rho$, the symbol duration $T_s$ can be expressed as:

$$T_s = \frac{N\rho}{2W}. \tag{5.14}$$

In addition, at T-R separation $d$ m, the UWB signal energy $E_s$ can be obtained by $E_s = P_r^u(d)T_s$. From (5.14), we have the channel symbol SNR $\gamma_0$ as following:

$$\gamma_0 = \frac{P_r^u(d)N\rho}{N_0W}. \tag{5.15}$$

Note that dimensionality parameter $N$ in (5.14) and (5.15) is $N = M$ for M-ary PPM and $N = 1$ for bi-phase and on-off keying signals. In order to investigate the trade off between the UWB capacity and the spreading ratio $\rho$, we express UWB capacities $\mathcal{C}^u_{\text{M-PPM}}$, $\mathcal{C}^u_{\text{on-off}}$ and $\mathcal{C}^u_{\text{bi-phase}}$ by substituting (5.14) and (5.15) into (5.7), (5.11) and (5.12) and obtain

$$\mathcal{C}^u_{\text{M-PPM}} = \frac{C_{\text{M-PPM}}(\gamma)}{T_s} = \frac{2W}{M\rho} C_{\text{M-PPM}}\left(\frac{P_r^u(d)M\rho}{N_0W}\right) \quad \text{[bits/s]}, \tag{5.16}$$

$$\mathcal{C}^u_{\text{on-off}} = \frac{C_{\text{on-off}}(\gamma)}{T_s} = \frac{2W}{\rho} C_{\text{on-off}}\left(\frac{P_r^u(d)\rho}{N_0W}\right) \quad \text{[bits/s]}, \tag{5.17}$$

$$\mathcal{C}^u_{\text{bi-phase}} = \frac{C_{\text{bi-phase}}(\gamma)}{T_s} = \frac{2W}{\rho} C_{\text{bi-phase}}\left(\frac{P_r^u(d)\rho}{N_0W}\right) \quad \text{[bits/s]}. \tag{5.18}$$

Based on above equations of capacities, as the example, we present the results for the UWB system operating at low band (3.1 GHz - 5.15 GHz). Fig. 5.7 shows the capacities of UWB over AWGN channel as the function of T-R separation $d$ when the spreading ratio $\rho = 5$, the capacities of UWB system utilizing M-ary PPM are compared with the capacity of the system with bi-phase and on-off keying. As we discussed before, $\rho = 5$ is the minimum value of the spreading ratio could be achieved by UWB signal under our assumptions on the system model, therefore Fig. 5.7 exhibits the UWB capacities for different modulation without spectrum spreading. In this scenario, the duty cycle of the UWB pulses are almost equal to $N$ ($N = M$ for M-ary PPM, $N = 1$ for bi-phase and on-off keying). Since the bandwidth $W$ are given from 3.1 GHz - 5.15 GHz and spreading ratio is a fixed value 5, Shannon bandwidth in Fig. 5.7 for different modulations are same, e.g., $B = W/5$. It can be observed that given Shannon bandwidth $B$, the system with 4-PPM will achieve the higher capacity (bits/s) than other M-ary PPM scheme when the UWB T-R distance is within 20 meters. It also can be shown that by given the same $B$, the capacities (bits/s) of UWB system utilizing on-off keying and bi-phase could be twice more than the capacity of the system with 4-PPM at the short distance ($d < 5$m).

The trade off between the UWB capacity and spreading ratio are illustrated in Fig. 5.8 and Fig. 5.9 for $d = 3$m and $d = 15$m respectively. Among the M-ary PPM capacity curves, the one for $M = 4$ always on the top which indicates the optimal $M$ for M-ary PPM UWB is $M^*_{opt} = 4$. From those two figures, it can be observed that reducing the spreading ratio can always bring the high capacity benefit for UWB system when the channel is modeled as AWGN. Since the spreading ratio $\rho$ is related to symbol duration $T_s$ given in (5.14) and $T_s = N_p T_f$ is defined in signal model in section 5.1, we have

$$T_f = \frac{M N_p \rho}{2W}. \tag{5.19}$$

Thus for an UWB system with the bandwidth $W$ and fixed $N_p$ (number of pulses modulated in one symbol, in this chapter we choose $N_p$ as the minimum integers than meet PRF $= N_p R_s > 1$MHz), the value of spreading ratio is determined by how close the transmitted pulses are adjacent to each other. Therefore, in AWGN channel, in order to obtain the higher capacity, the UWB pulses should be placed as close as possible, as long as the corresponding spreading ratio meet the system requirement. However this situation is not always true over the multipath channel. Due to the delay spread from channel responds, the sequence of pulses are received from single pulse transmission. Intuitively, the interference will happen when the pulse frame time $T_f$ is less than the maximum delay spread of the channel. Such interference can be classified into two kinds. One is called inter-symbol-interference (ISI) which is caused by delay spread of previous pulses belonged to the prior symbols. Still, in multipath channel, transmitting the pulse more close can result in the lower spreading ratio, hence result in the higher capacity. On the other hand, the possible ISI due to $T_f < T_m$ could reduced the capacity of UWB system. In following section, the UWB capacity will be studied for multipath channel. The trade off between the spreading ratio and UWB capacity is expected to be different over multipath channel.

## 5.3 Capacity of UWB Systems over Multipath Channel

Due to the delay spread effect of the channel, if $T_s < T_m$, when the current transmitted signal $S_i(t)$ given in (5.1) pass through the multipath channel modeled as in (3.6), the received signal $r(t)$ is not only the output of the channel corresponding to $S_i(t)$, but also depended on the previous transmitted signals. If we denote $N_v = \text{floor}(T_m/T_s)$, the $v^{th}$ $(v = \pm 1, \pm 2, \ldots, \pm N_v)$ transmitted signal $S_{i(v)}(t)$, which could cause ISI to the current signal $S_i(t)$, can be expressed as

$$S_{i(v)}(t) = \sum_{n=0}^{N_p-1} a_{i(v)} \sqrt{E_p} p(t - b_{i(v)} T_{PPM} - nT_f). \tag{5.20}$$

Thus the received signal $r(t)$ is generated as:

$$\begin{aligned} r(t) &= S_i(t) * h(t) + \sum_{v=-N_v, v\neq 0}^{N_v} S_{i(v)}(t) * h(t + vT_s) + n(t) \\ &= \sum_{n=0}^{N_p-1} a_i \sqrt{E_p} g(t - b_i T_{PPM} - nT_f) \\ &\quad + \sum_{\nu=-N_v, v\neq 0}^{N_v} \sum_{n=0}^{N_p-1} a_{i(v)} \sqrt{E_p} g(t - b_{i(v)} T_{PPM} - nT_f + vT_s + n(t), \quad (5.21) \end{aligned}$$

where $n(t)$ is AWGN noise with zero mean and PSD $N_0/2$. $g(t)$ is the output of UWB pulse $p(t)$ through channel $h(t)$, given as

$$g(t) = p(t) * h(t) = \sum_{k=1}^{K} h_k p(t - \tau_k). \quad (5.22)$$

Note that the duration of signal $g(t)$ is $T_g = T_m + T_p$.

### 5.3.1 Performance of Rake Receiver

The Rake receiver is employed to detect the signals in a multipath environment. Following analysis is performed for the general $L$-tap Rake receiver.

Denote the delay for $L$-tap Rake receiver as $\theta_l, l = 0, ..., L-1$, and $0 < \theta_0 < \theta_1 < ... < \theta_L - 1 < T_m$. The Rake receiver can be modeled as the tapped delay-line model and is performing cross-correlation with the reference signals at the $L$-tap delay. The reference signal $\phi_j(t)$ corresponding to the input signal $S_j(t)$ in (5.1) is given by

$$\phi_j(t) = \frac{1}{\sqrt{N_p}} \sum_{n=0}^{N_p-1} a_j p(t - b_j T_{PPM} - nT_f). \quad (5.23)$$

Denote $y_{j,l|i}$ as the output of the $j$th correlator corresponding to the $l$th finger of the Rake receiver when the transmitted signal is $i$th symbol stream $S_i(t)$, we have

$$\begin{aligned} y_{j,l|i} &= \int_{-\infty}^{\infty} r(t)\phi_j(t - \theta_l)dt \\ &= \int_{-\infty}^{\infty} \left( S_i(t) * h(t) + \sum_{v=-N_v, v\neq 0}^{N_v} S_{i(v)}(t) * h(t + vT_s) \right) \phi_j(t - \theta_l)dt \end{aligned}$$

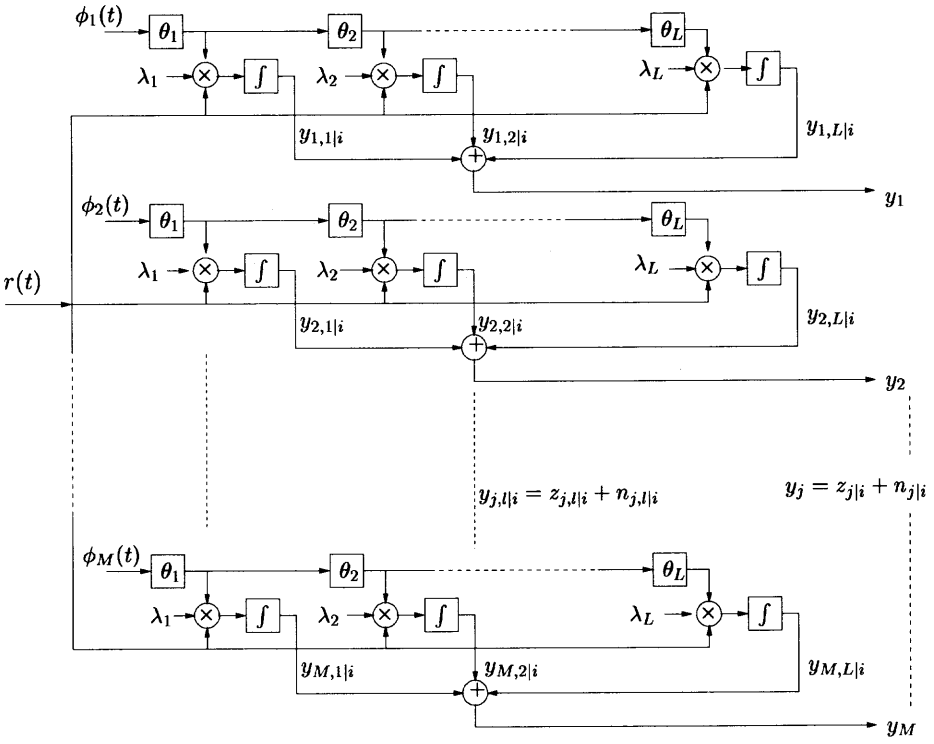


**Figure 5.2** L-tap Rake receiver.

$$
\begin{aligned}
&+ \int_{-\infty}^{\infty} n(t)\phi_j(t-\theta_l)dt \\
&= x_{j,l|i} + z_{j,l|i} + n_{j,l|i}.
\end{aligned} \tag{5.24}
$$

By defining $\alpha_{gp}(\tau)$ is the cross correlation function between $p(t)$ and $g(t)$ as

$$
\alpha_{gp}(\tau) = \int_{-\infty}^{\infty} g(t)p(t-\tau)dt, \tag{5.25}
$$

the signal component $x_{j,l|i}$ and ISI component $z_{j,l|i}$ in (5.24) can be expressed as

$$
x_{j,l|i} = \sqrt{\frac{E_p}{N_p}} \sum_{n=0}^{N_p-1} \sum_{m=0}^{N_p-1} a_i a_j \alpha_{gp}[(b_j - b_i)T_{PPM} - (n-m)T_f + \theta_l], \tag{5.26}
$$

$$
z_{j,l|i} = \sqrt{\frac{E_p}{N_p}} \sum_{v=-N_v, v\neq 0}^{N_v} \sum_{n=0}^{N_p-1} \sum_{m=0}^{N_p-1} a_{i(v)} a_j \alpha_{gp}[(b_j - b_{i(v)})T_{PPM} - (n-m)T_f + vT_s + \theta_l]. \tag{5.27}
$$

where $\alpha_{gp}(\tau) = 0$ when $\tau \leq -T_p$ or $\tau \geq T_g$. The noise part $n_{j,l|i}$ of the output Rake finger is zero mean Gaussian random variables with the variance $\sigma_0^2 = N_0/2$.

Several combining techniques are employed in Rake receiver to combine the detected multipath components. Among them, the optimum combiner is the maximal ratio combiner (MRC). By using MRC, the output signal-to-noise ratio (SNR) at the Rake receiver is the sum of the SNRs of each individual diversity branch [19], which yields the maximum output SNR comparing with other combining technique. The weight for the $l$th tap finger output $\lambda_l$ can be estimated from the receiver's knowledge of the channel.

In this paper, channel information is assumed perfectly known at the receiver, thus the delay of $L$-tap Rake receiver $\theta_l$ and the weights of the MRC can be estimated perfectly, e.g., $\lambda_l = h_k$ when $\theta_l = \tau_k$, for $l = 1, 2, .., L$ and $k = 1, 2, ..., K$. If we denote the Rake receiver parameter $\{\theta_l, \lambda_l\}$ as $\underline{\Lambda}$, and the channel information $\{\tau_k, h_k\}$ as $\underline{\Omega}$, we have $\underline{\Lambda} \in \underline{\Omega}$.

Finally, the output of the Rake receiver after MRC is $y_j, j = 1, 2, \ldots, M$, given by

$$\begin{aligned} y_j &= \sum_{l=0}^{L-1} \lambda_l y_{j,l|i} = \sum_{l=0}^{L-1} \lambda_l x_{j,l|i} + \sum_{l=0}^{L-1} \lambda_l z_{j,l|i} + \sum_{l=0}^{L-1} \lambda_l n_{j,l|i} \\ &= x_{j|i} + z_{j|i} + n_{j|i}, \end{aligned} \tag{5.28}$$

where $n_{j|i}$ is the Gaussian random variables with zeros mean and variance $\sigma_n^2 = \sum_{l=0}^{L-1} \lambda_l^2$. $x_{j|i}$ in (5.28) is the combined signal components which has following expression

$$x_{j|i} = \sqrt{\frac{E_p}{N_p}} \sum_{l=0}^{L-1} \lambda_l \left( \sum_{n=0}^{N_p-1} \sum_{m=0}^{N_p-1} a_i a_j \alpha_{gp}[(b_j - b_i)T_{PPM} - (n-m)T_f + \theta_l] \right), \tag{5.29}$$

and the combined ISI components is

$$z_{j|i} = \sqrt{\frac{E_p}{N_p}} \sum_{l=0}^{L-1} \lambda_l \left( \sum_{v=-N_v, v\neq 0}^{N_v} \sum_{n=0}^{N_p-1} \sum_{m=0}^{N_p-1} a_{i(v)} a_j \alpha_{gp}[(b_j - b_{i(v)})T_{PPM} - (n-m)T_f + vT_s + \theta_l] \right). \tag{5.30}$$

We define $\xi = (b_j - b_{i(v)})T_{PPM} - (n-m)T_f + vT_s + \theta_l$, from the definition of signal $\alpha_{gp}(\tau)$ in (5.25), it can be assured no ISI will occur if $\xi < -T_p$ or $\xi > T_g$. Since the value of $\xi$ is jointly determined by several factors, it is hard to predict the occurrence of ISI. In Appendix, we provide a sufficient but not necessary condition for no ISI. This sufficient condition states that when M-ary PPM UWB signal pass through the multipath channel with the maximum delay spread $T_m$, if the pulse frame time $T_f$ is larger than $M(T_m + T_p)$, no ISI will happen for such UWB system. Accordingly, the condition of no ISI for bi-phase and on-off keying modulated UWB system is $T_f \geq T_m + T_p$.

In addition to ISI, for M-ary PPM, these are another type of interference could be harmful to the system. This kind of interference is hidden in the desired signal part $x_{j|i}$ and will happen when $\alpha_{gp}[(b_j - b_i)T_{PPM} + \theta_l] \neq 0$ for $b_j \neq b_i$. Ideally, despite of ISI, the desired signal output of the $j$th correlator for the $i$th transmitted signal should be zero when $i \neq j$, due to orthogonality between the reference signal $\phi_i(t)$ and the signal part in received signal $r(t)$. However this orthogonality could be destroyed by the delay spread of the multipath channel, resulting in an interference. This type of interference is named as self-interference (SI) to distinguish it from ISI. In Appendix, for system using M-ary PPM, the sufficient condition for no SI is shown identical to the condition for no ISI. Apparently, no SI will happen for bi-phase and on-off keying modulated system.

In this thesis, ISI component $z_{j|i}$ is assumed as a Gaussian random variable with zero mean and variance $\sigma_z^2$. The value of the $\sigma_z^2$ is depend on the multipath

channel parameter characteristic as well as the symbol time $T_s$. We also assume ISI component $z_{j|i}$ and AWGN noise $n_{j|i}$ are two i.i.d. random variables. From above analysis, conditional on the channel information $\underline{\Omega}$, the output of the $j$th correlator corresponding to the $i$th signal input $y_j$ can be regarded as a Gaussian random variables as

$$y_j \text{ is } \mathcal{N}(x_{j|i}, \sigma_z^2 + \sigma_n^2) \quad i, j = 1, \ldots, M. \tag{5.31}$$

Note that the result of $y_j$ in (5.31) is suitable for M-ary PPM, bi-phase and on-off keying. Due to ISI and SI (only for PPM), the output $y_j$ in (5.31) are random variables and has the different distribution with $y_j$ in (5.6) and (5.13) for AWGN channel. Thus, capacities for M-ary PPM, bi-phase and on-off keying signals over the multipath channel may only evaluated by the M-ary capacity expression in (5.5), the simplified expressions for AWGN channel in (5.7), (5.11) and (5.12) can not be used for the multipath channel. Conditioning upon channel information $\underline{\Omega}$, we denote $C_{\text{M-ary}}(\mathbf{Y}; \mathbf{S} \mid \underline{\Omega})$ as the conditional capacity (bits/symbol) for M-ary signal over the multipath channel. The numerical result of $C_{\text{M-ary}}(\mathbf{Y}; \mathbf{S} \mid \underline{\Omega})$ can be obtained from (5.5) by substituting $p(\mathbf{Y} \mid \mathbf{s}_j)$ with conditional pdf $p(\mathbf{Y} \mid \mathbf{s}_j, \underline{\Omega})$, which can be expressed as

$$p(\mathbf{Y} \mid \mathbf{s}_i, \underline{\Omega}) = \left( \frac{1}{2\pi(\sigma_z^2 + \sigma_n^2)} \right)^{M/2} \prod_{j=1}^{M} \exp\left[ \frac{(y_j - x_{j|i})^2}{2(\sigma_z^2 + \sigma_n^2)} \right]. \tag{5.32}$$

In addition, the UWB pulse energy $E_p$ in $x_{j|i}$ of (5.30) is $E_p = E_s/N_p$ and $E_s$ can be obtained by $E_s = P_r^u(d)T_s$. The symbol time $T_s$ is related to spreading ratio as in (5.14), therefore, we get the conditional capacity (bit/s) subject to UWB constraints over the multipath channel as following:

$$\mathcal{C}^u_{\text{M-ary}}(\mathbf{Y}; \mathbf{S} \mid \underline{\Omega}) = \frac{2W}{N\rho} C_{\text{M-ary}}(\mathbf{Y}; \mathbf{S} \mid \underline{\Omega}) \text{ [bits/s]}. \tag{5.33}$$

### 5.3.2 Outage Capacity

The conditional capacity $C^{u}_{\text{M-ary}}(\mathbf{Y};\mathbf{S} \mid \underline{\Omega})$ (bits/s)in previous sections was calculated based on single channel realization. Due to the multipath channel fading, the channel parameter $\underline{\Omega}$ are random variables at the different channel realizations. Therefore the information theoretic capacities over the multipath channel are also random variables when the fading effect are considered. Capacities can be characterized by their complementary cumulative distribution functions (CCDF). In turn, numerical CCDFs can be evaluated empirically from Monte-Carlo simulations.

The above analysis of the capacity for multipath channel is performed for the general $L$-tap rake receiver. In [22], an all Rake (ARake) receiver was defined as the receiver with unlimited number of correlators. Since we assume the channel information is perfectly known at the receiver, parameter of ARake $\underline{\Lambda}$ will be identical to channel information $\underline{\Omega}$, such that, theoretically it combines all of the resolved multipath components. Since $\sum_{k=1}^{K} h_k^2 = 1$ is assumed in the multipath channel model, the results for ARake are identical to the AWGN. Alternatively, the receiver may employ a selective Rake (SRake) receiver, which combines only the $L$ strongest paths.

In Fig. 5.10 and Fig. 5.11, the 10% outage capacity of SRake with $L = 20$ are plotted as function of distance $d$ with spreading ratio $\rho = 1$ and $\rho = 5$ respectively. In both figures, the capacities of UWB system employing 4-PPM (for $M^{*}_{opt} = 4$), on-off keying and bi-phase are compared. The UWB system performs in low band (3.1 GHz - 5.15 GHz) and the transmitted power is subject to the FCC PSD limitation. The UWB capacity for AWGN channel, also showed in Fig. 5.10 and Fig. 5.11 as a comparison,

Furthermore, as a function of spreading ratio $\rho$, the 10% outage capacity for the SRake with $L = 20$ are shown in Fig. 5.12 and Fig. 5.13.

## 5.4 Chapter Summary

In this chapter, we compute channel capacity of M-ary PPM UWB communications for the AWGN and multipath channels.

Starting from the known capacity of PPM orthogonal signals, the computation of UWB capacity for the AWGN channel takes into account UWB specific constraints. The constraints are the power spectrum density limitation under FCC Part 15 rules and the spreading ratio required to achieve a specified jam resistance level. UWB capacity in AWGN channel is expressed as a function of spreading ratio and communication range. Trade-offs between capacity and range of communications and between capacity and spreading ratio are explored. We also compute the capacity of UWB system over the multipath channel. By assuming the channel information is perfectly known at the receiver, the complementary cumulative distribution function (CCDF) of the capacities are obtained for ARake receiver and SRake receiver. In both cases, MRC is employed. Similar as the capacity over AWGN channel, outage capacity (such as 10% outage) of the UWB system over the multipath channel are illustrated as a function of spreading ratio and communication range subject to the FCC PSD limitation.

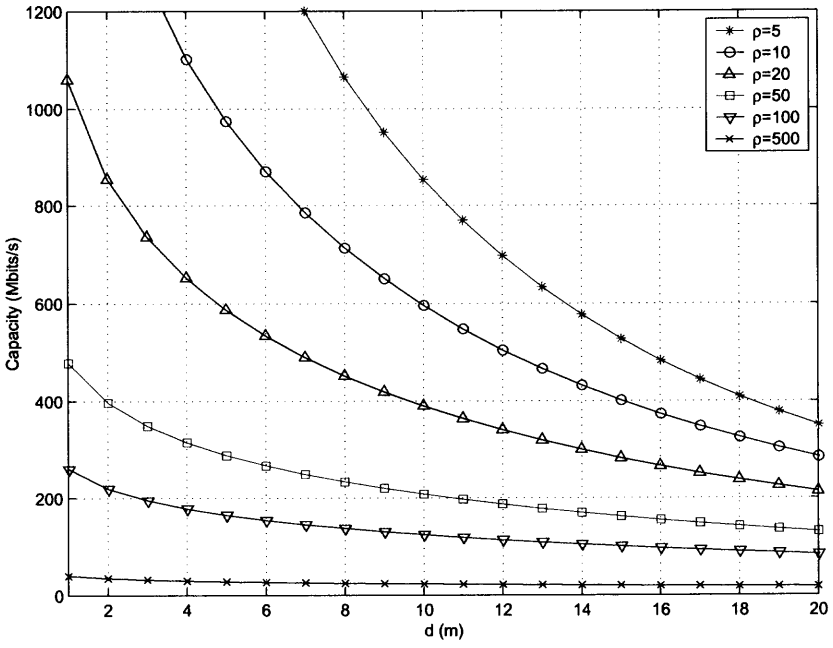


**Figure 5.3** Shannon capacity for UWB system with the bandwidth from 3.1 GHz to 5.15 GHz.

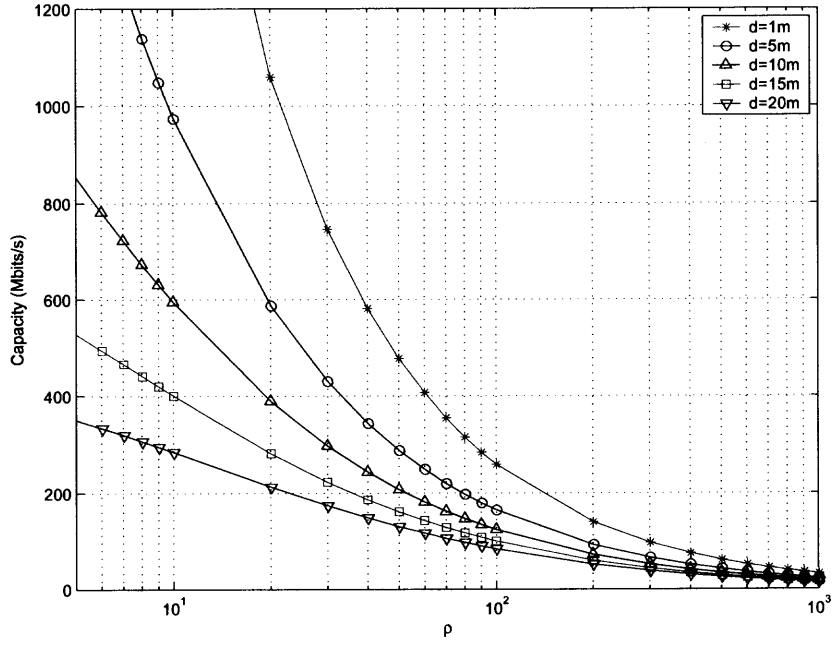


**Figure 5.4** At the distance d, the trade off between the Shannon capacity with the spreading ratio, UWB system has the bandwidthfrom 3.1 GHz to 5.15 GHz.

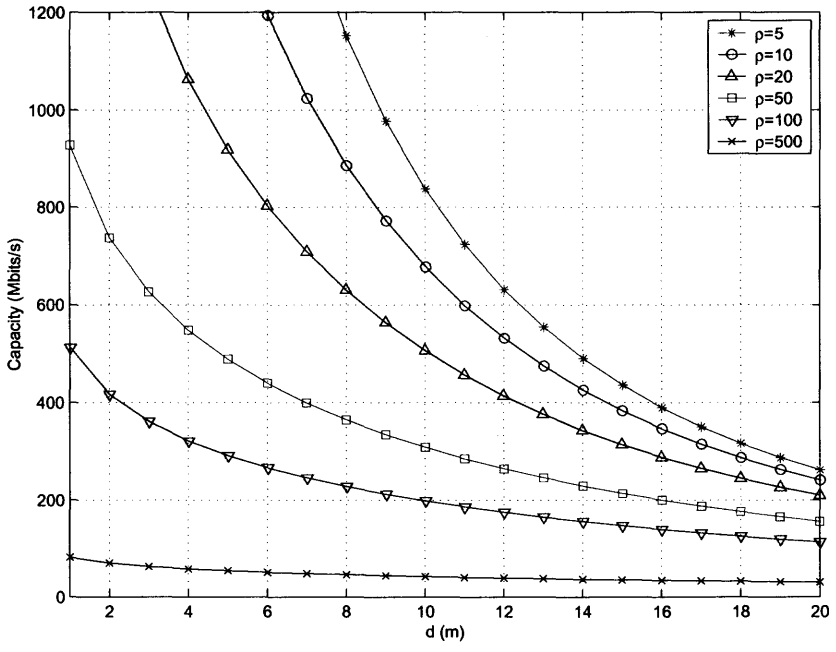


**Figure 5.5** Shannon capacity for UWB system with the bandwidth from 5.825 GHz to 10.6 GHz.

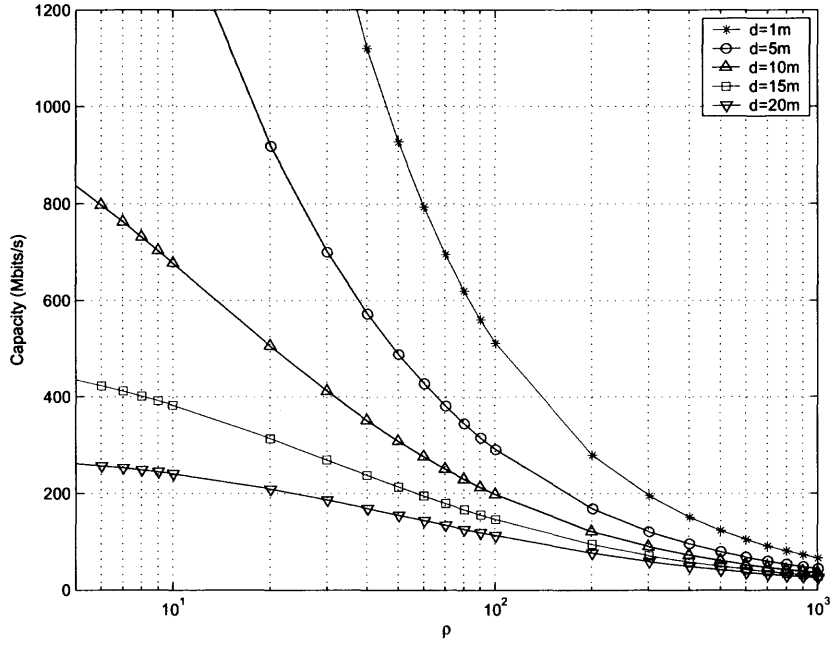


**Figure 5.6** At the distance d, the trade off between the Shannon capacity with the spreading ratio, UWB system has the bandwidthfrom 5.825 GHz to 10.6 GHz.

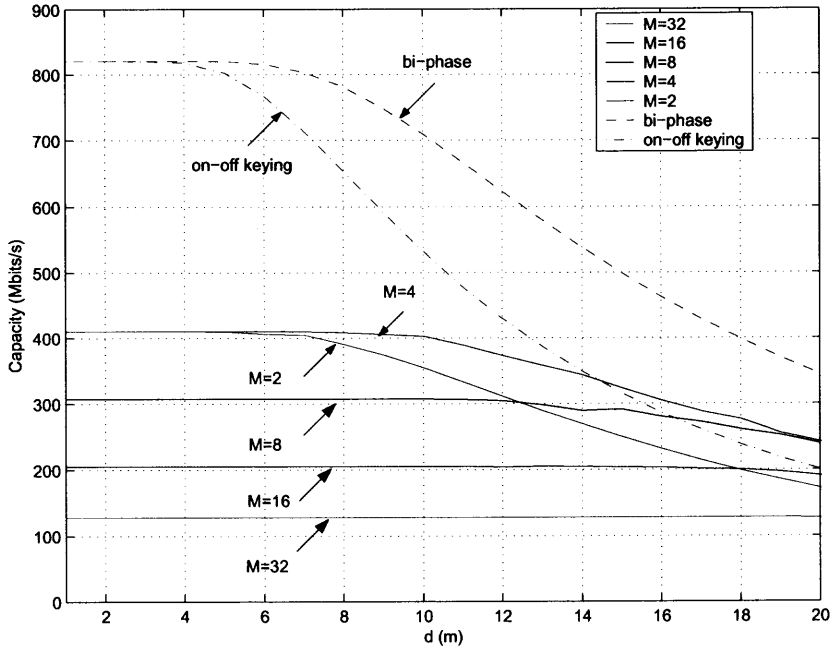


**Figure 5.7** M-ary PPM, bi-phase and on-off keying capacity with the spreading ratio $\rho = 5$.

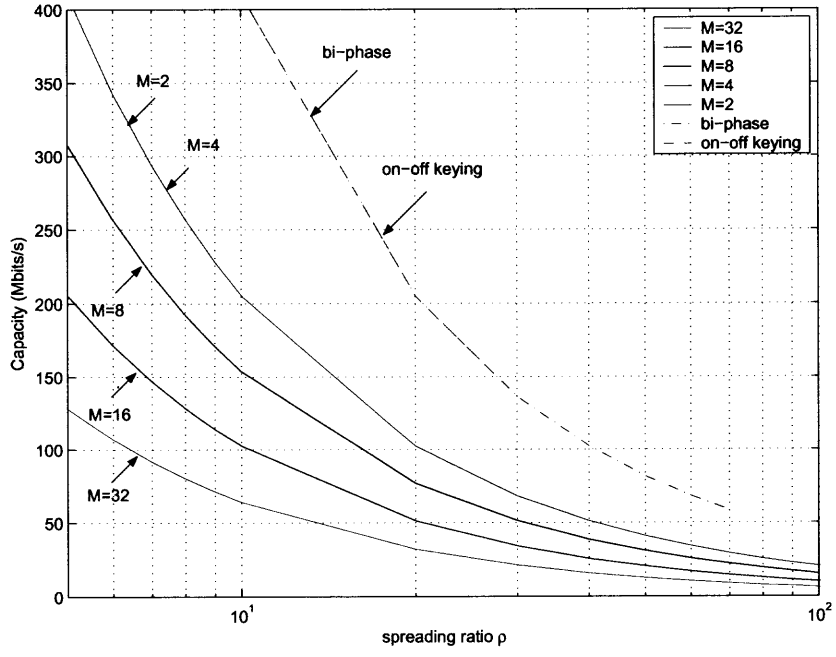


**Figure 5.8** At the distance d=3m, the trade off between the M-ary PPM, bi-phase and on-off keying capacity with the spreading ratio.

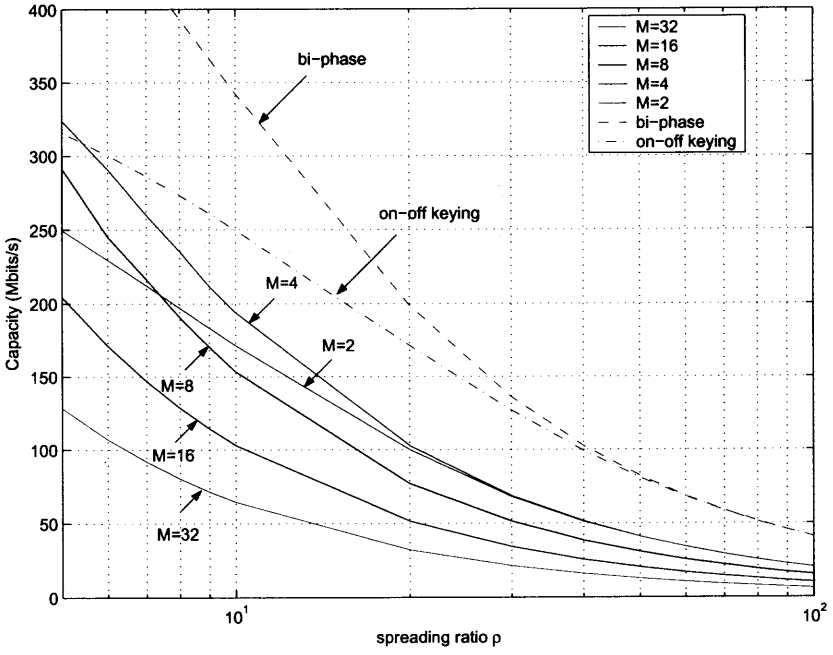


**Figure 5.9** At the distance d=5, the trade off between the M-ary PPM, bi-phase and on-off keying capacity with the spreading ratio.

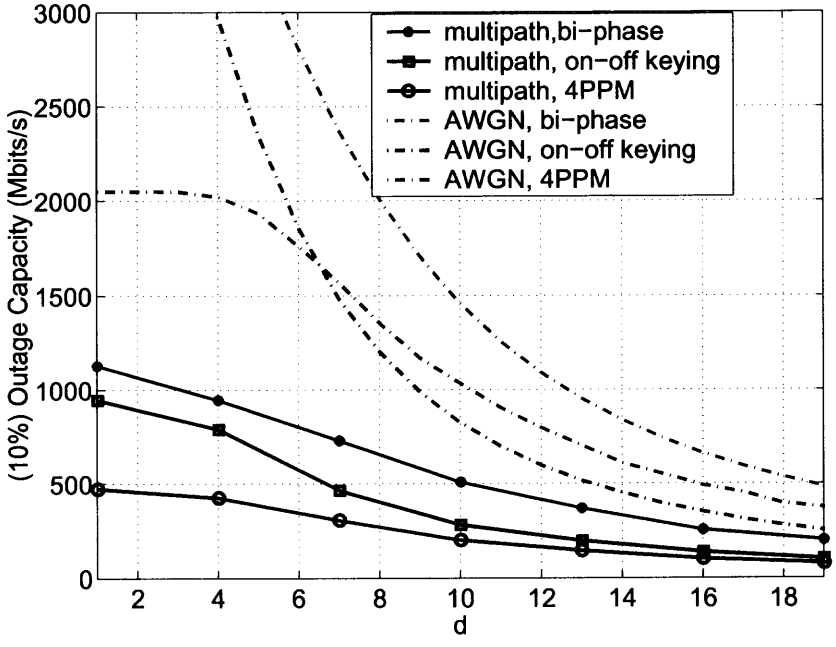


**Figure 5.10** Outage capacity for 4-PPM, bi-phase and on-off keying, spreading ratio $\rho = 1$, the SRake L=20 is employed.

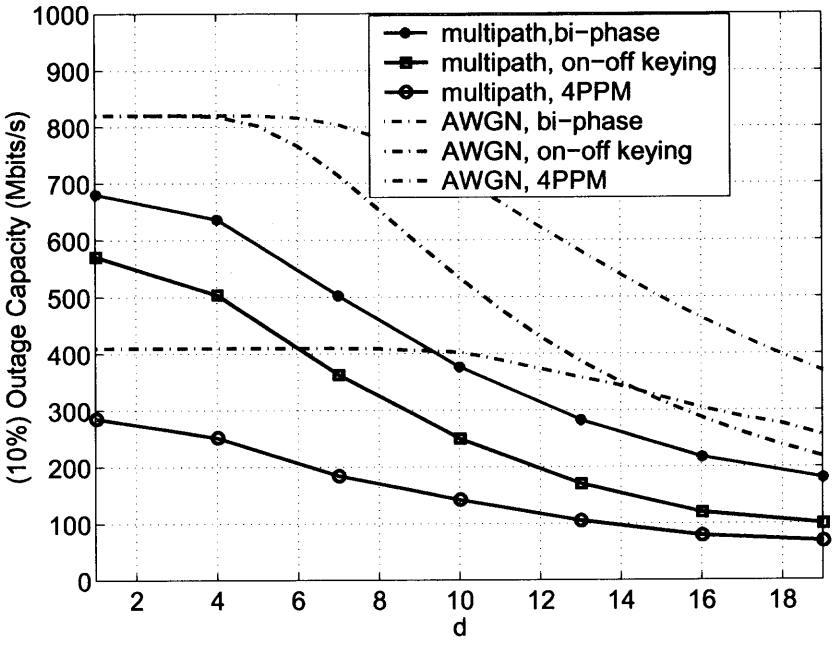


**Figure 5.11** Outage capacity for 4-PPM, bi-phase and on-off keying, spreading ratio $\rho = 5$, the SRake L=20 is employed.

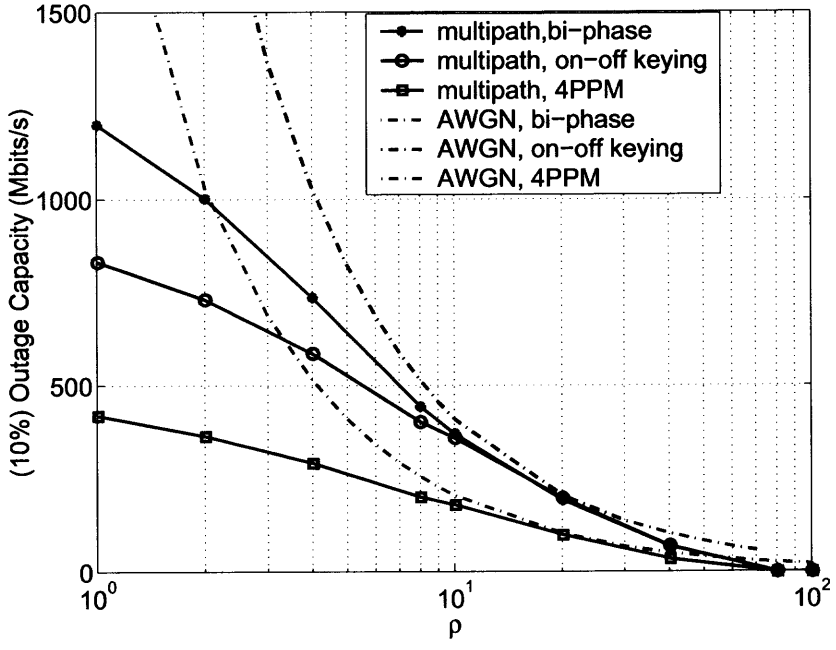


**Figure 5.12** At the distance $d = 3$ m, the trade off between the 4-PPM, bi-phase and on-off keying capacity with the spreading ratio, the SRake L=20 is employed.

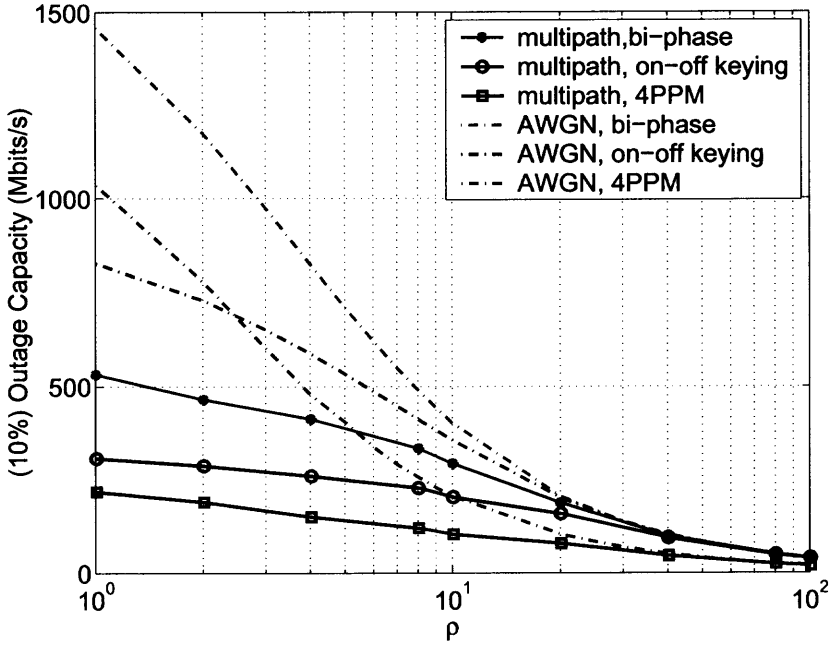


**Figure 5.13** At the distance $d = 10$ m, the trade off between the 4-PPM, bi-phase and on-off keying capacity with the spreading ratio, the SRake L=20 is employed.

# CHAPTER 6

# CAPACITY OF UWB MULTIPLE-ACCESS SYSTEMS

Time-hopping is used in UWB to as a multiple-access method. In this case, the inter-user interference will be the factor limiting communications. Some published work has addressed the issue of how many users can the UWB channel support [24, 25]. This work demonstrates the trade off between the achievable data rate, bit error probability (BEP) and the number of users. In this chaptert, the results in [25] and [26] will be extended in several ways: (1) compute the information theoretic capacity of an UWB multiuser system subject to the specific pulse waveform, (2) consider M-ary PPM.

In this chapter, the channel capacity of M-ary PPM UWB communications over multiple-access channels is computed. The capacity for multiple-access channels is derived from SNR considerations. A certain SNR is required to achieve a specified bit error probability (BEP). The noise floor raises with the number of users. We assume UWB transmissions utilizing a rectangular pulse. It should be mentioned that the same analysis can be extended to other practical waveforms.

This chapter is organized as follows. It begin with multiple-access UWB systems model in section 6.1. Analysis of M-ary PPM UWB capacity for multiple-access system is carried out in section 6.2. Finally, conclusions and future works are provided in section 6.3.

## 6.1 Multiple-Access UWB Systems Model

The time-hopping M-ary PPM system model examined in this paper is similar to that used in [27, 28] and it is shown in Fig. 6.1. The $\nu$-th ($1 \leq \nu \leq N_u$) user's transmitted

signal has the form:

$$S^{(\nu)}(t) = \sum_{n=0}^{N_p-1} A^{(\nu)}\, p(t - c_n^{(\nu)} T_c - d_n^{(\nu)} - nT_f), \tag{6.1}$$

where $A^{(\nu)} = \sqrt{E_p^{(\nu)}}$, $c_n^{(\nu)}$ and $d_n^{(\nu)}$ are respectively, the amplitude, time-hopping, and modulation for user $\nu$. We have $d_n^{(\nu)} \in \{\delta_1, \ldots, \delta_M\}$. Other symbols have the same meaning as defined in the signal model in Chapter 2.

To simplify the analysis of UWB multi-user capacity, we assume a rectangular pulse. This analysis can be extended to other waveforms. The number of pulses in each symbol, $N_p$, is assumed to be 1.

The received signal $R(t)$ from all users is given by:

$$R(t) = \sum_{\nu=1}^{N_u} S^{(\nu)}(t - \tau^{(\nu)}) + n(t), \tag{6.2}$$

where $\tau^{(\nu)}$ is the time delay associated with user $\nu$ and $n(t)$ is zero-mean AWGN with power spectral density $N_0/2$.

Without loss generality, we assume the desired user is $\nu = 1$. The optimal receiver for single-user UWB signal is the M-ary pulse correlation receiver followed by a detector, as shown in Fig. 6.2. We assume the receiver is perfectly synchronized to user 1, i.e., $\tau^{(1)}$ is known. Furthermore, the time hopping sequence $c_n^{(1)}$ is known at the receiver. The M-ary correlation receiver for user 1 consists of $M$ filters matched to the basis functions $\phi_i^{(1)}(t)$ defined as:

$$\phi_i^{(1)}(t) = p(t - \delta_i - \tau^{(1)}), \;\; i = 1, .., M. \tag{6.3}$$

At sample time $t = nT_f$, the output of each filter, $y_i$, $i = 1, .., M$, is:

$$y_i = \int_{(n-1)T_f}^{nT_f} R(t)\phi_i^{(1)}(t - nT_f - c_n^{(1)})dt, \tag{6.4}$$

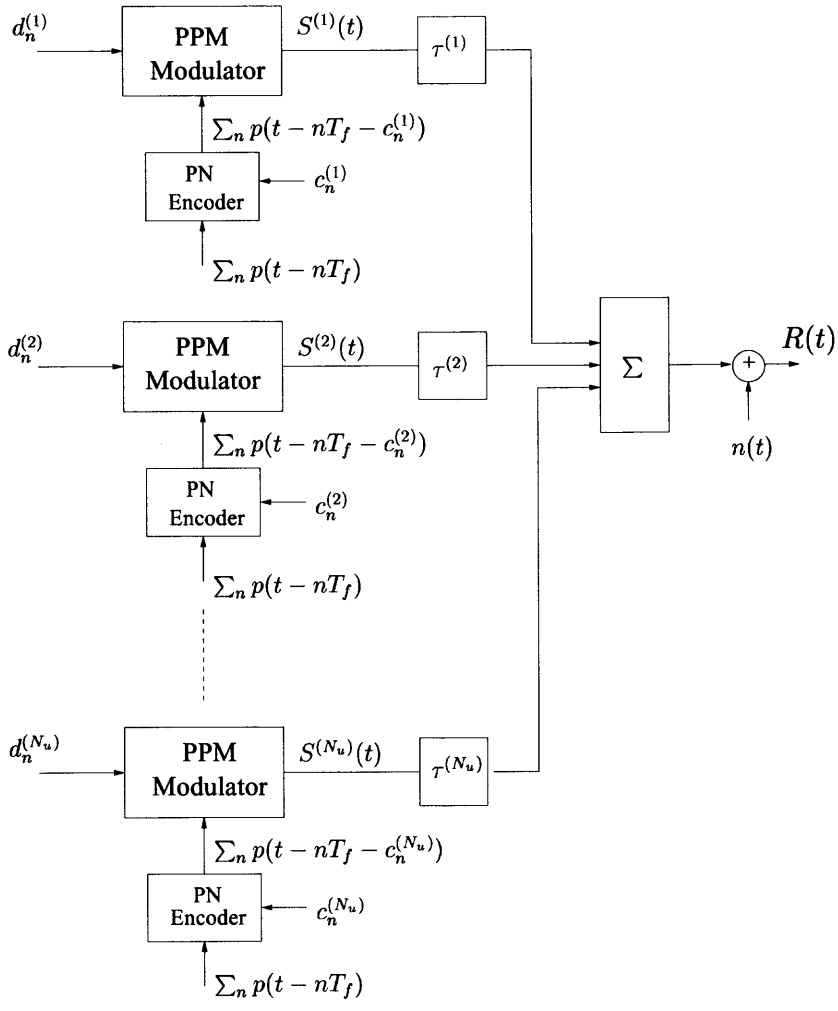


**Figure 6.1** Time-hopping M-ary PPM UWB multiple-access system model.

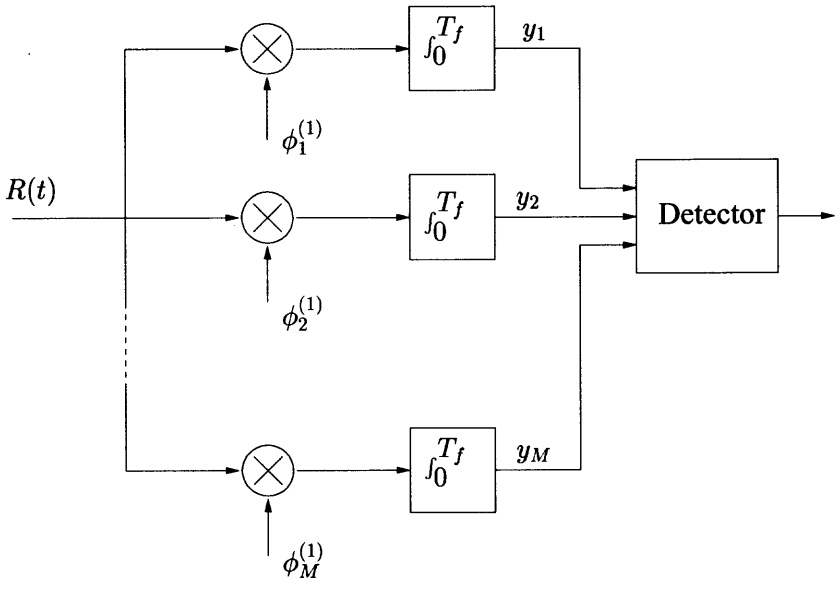


**Figure 6.2** UWB receiver for user 1.

which can be put in the form:

$$y_i = \begin{cases} A^{(1)} + N_I + N & \text{signal} \\ N_I + N & \text{no signal,} \end{cases} \tag{6.5}$$

where $N_I$ and $N$ are respectively, the multiple-access interference (MAI) and AWGN. We have

$$N_I = \sum_{\nu=2}^{N_u} \int_{(n-1)T_f}^{nT_f} A^{(\nu)} p(t - nT_f - c_n^{(\nu)} T_c - \delta_n^{(\nu)} - \tau^{(\nu)}) \phi_i^{(1)}(t - nT_f - c_n^{(1)}) dt, \tag{6.6}$$

and

$$N = \int_{(n-1)T_f}^{nT_f} n(t) \phi_i^{(1)}(t - nT_f - c_n^{(1)}) dt. \tag{6.7}$$

For any pulse $p(t)$ with duration $T_p$, we define the correlation $h(\Delta)$:

$$h(\Delta) = \int_0^{T_f} p(t) p(t - \Delta) dt. \tag{6.8}$$

Then the MAI component in (6.6) can be written

$$N_I = \sum_{\nu=2}^{N_u} A^{(\nu)} h(\Delta), \tag{6.9}$$

where $\Delta$ is the time difference between users 1 and $\nu$. The time difference $\Delta$ can be expressed:

$$\Delta = (c_n^{(1)} - c_n^{(\nu)})T_c - (d_n^{(1)} - d_n^{(\nu)}) - (\tau^{(1)} - \tau^{(\nu)}). \tag{6.10}$$

To provide a statistical characterization of $\Delta$, the following assumption are made:

1. The time-hopping code elements $c_n^{(\nu)}$ are random, independent, identically distributed (i.i.d.) with a uniform distribution over the frame interval $T_f$, for $\nu = 1, ..., N_u$ and for all $j$.

2. Each user $\nu$ has a uniform distributed data source, such that the probability of any $M$-ary PPM symbol is $1/M$. We further assume that the data sequences corresponding to all users consist of independent symbols. Hence the corresponding time shifts $d_n^{(\nu)}$ are also independent identically distributed (i.i.d.) random variables.

3. The time delays $\tau^{(\nu)}$ are also assumed random, i.i.d uniformly distributed over the frame interval.

Under the assumptions listed above, and noting that MAI pulses of interest fall within the same UWB frame, the time difference $\Delta$ is a random variable uniformly distributed over the interval $[-T_f, T_f]$. This interval allows to accommodate also $\Delta$ with negative sign. At the output of user 1's receiver, the distribution of the MAI component $N_I$ depends on the statistical characteristics of $\Delta$. Strictly speaking, the multiple-access interference $N_I$ is not Gaussian. However, by assuming perfect power control, we make the Gaussian assumption for the MAI $N_I$ by invoking the central limit theorem for a sufficiently large number of users $N_u$.

From (6.5), the output of the sampler at user 1's receiver consists of independent Gaussian random variables $y_i$ distributed as follows:

$$\begin{array}{lll} y_i \text{ is } \mathcal{N}(A^{(1)} + E[N_I],\ \sigma_I^2 + N_0/2) & \text{signal} \\ y_i \text{ is } \mathcal{N}(E[N_I],\ \sigma_I^2 + N_0/2) & \text{no signal,} \end{array} \tag{6.11}$$

where $E[N_I]$ and $\sigma_I^2$ are respectively, the mean and variance of $N_I$.

## 6.2 Capacity of UWB Multiple-Access Systems

Consider a UWB system utilizing a rectangular waveform. The UWB pulse $p_{re}(t)$ is expressed as in (2.1).

Then the correlation function for rectangular pulse waveform $p_{re}(t)$ in (2.1) is given by:

$$h(\tau) = 1 - \frac{|\tau|}{T_p}, \quad 0 \le |\tau| \le T_p. \tag{6.12}$$

As justified earlier, the time shift difference between users $\Delta$ defined in (6.10) is modeled with a uniform distribution over the interval $[-T_f, T_f]$. It follows that the probabilities $P(-T_p \le \Delta \le 0) = P(0 \le \Delta \le T_p) = T_p/(2T_f) = 1/(2\beta)$. It is noted that the parameter $\beta$ serves in the measurement of the probability of $\Delta$ falling in the interval $[-T_p, T_p]$. From (6.12), the mean value of $h(\Delta)$ can be calculated as follows:

$$\begin{aligned} E[h(\Delta)] &= E\left[h(\Delta)| -T_p \le \Delta \le 0\right] P(-T_p \le \Delta \le 0) \\ &+ E[h(\Delta)|0 \le \Delta \le T_p] P(0 \le \Delta \le T_p) \\ &= \frac{1}{2\beta}. \end{aligned} \tag{6.13}$$

The variance of $h(\Delta)$ is denoted $\sigma_h^2$. Since $E[h(\Delta)] = 1/(2\beta)$, we have

$$\begin{aligned} \sigma_h^2 &= E[h^2(\Delta)] - \left(\frac{1}{2\beta}\right)^2 \\ &= E[h^2(\Delta)| -T_p \le \Delta \le 0] P(-T_p \le \Delta \le 0) \end{aligned} \tag{6.14}$$

$$+E[h^2(\Delta)|0 \leq \Delta \leq T_p]P(0 \leq \Delta \leq T_p) - \frac{1}{4\beta^2}$$

$$= \frac{1}{3\beta} - \frac{1}{4\beta^2}. \tag{6.15}$$

For typical values of $\beta > 10$, we can approximate

$$\sigma_h^2 \approx \frac{1}{3\beta}. \tag{6.16}$$

Finally, the variance of the MAI term $N_I$ is:

$$\sigma_I^2 = \sum_{\nu=2}^{N_u} A^{(\nu)^2} \sigma_h^2 = \frac{\sum_{\nu=2}^{N_u} A^{(\nu)^2}}{3\beta}. \tag{6.17}$$

Taking into account the AWGN, the SNR per symbol at the output of the correlation receiver is given by

$$\gamma_I = \frac{A^{(1)^2}}{\sigma_I^2 + N_0/2} = \frac{A^{(1)^2}}{\left(\sum_{\nu=2}^{N_u} A^{(\nu)^2}/3\beta\right) + N_0/2}. \tag{6.18}$$

With perfect power control, $A^{(1)} = A^{(\nu)} = \sqrt{E_p}$, $\gamma_I$ becomes:

$$\gamma_I = \frac{3\beta}{(N_u - 1) + 3\beta/\gamma_0}, \tag{6.19}$$

where $\gamma_0 = 2E_p/N_0$. Since for M-ary PPM, the parameter $\beta$ is related to spreading ratio $\rho$ as $\beta = (M/2c)\rho$, with $c = 1$ (time-bandwidth product of the rectangular pulse), we have $\beta = (M/2)\rho$ in this case. Thus $\gamma_I$ can be written as:

$$\gamma_I = \frac{3M\rho}{2\,(N_u - 1) + 3M\rho/\gamma_0}. \tag{6.20}$$

From this expression, it can be observed that for a low number of users, the performance is noise limited. Conversely, for a number of users $N_u > (3M)\rho/(2\gamma_0)$, the performance increasingly becomes interference limited.

The multiple-access channel is modeled as an AWGN channel with two-sided noise spectral density $\sigma_I^2 + N_0/2$. Similar as the capacity of AWGN channel as in

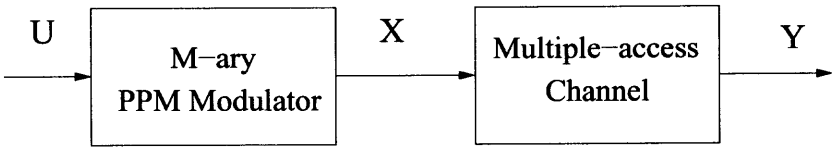


**Figure 6.3** UWB multiple-access channel model.

(5.7), the capacity of multiple-access channel as a function of the channel symbol SNR $\gamma_I$ , $C_{M-PPM}(\gamma_I)$, is given by [10]

$$C_{M-PPM}(\gamma_I) = \log_2 M - E_{\mathbf{v}|\mathbf{x}_1} \log_2 \sum_{m=1}^{M} \exp\left[\sqrt{\gamma_I}(v_m - v_1)\right] \quad \text{[bits/symbol]}, \quad (6.21)$$

where the random variables $v_m$, $m = 1, .., M$ have the following distribution:

$$\begin{aligned} v_1 \quad & \text{is} \quad \mathcal{N}(\sqrt{\gamma_I}, 1) \\ v_m \quad & \text{is} \quad \mathcal{N}(0, 1) \quad m \neq 1. \end{aligned}$$

For given bandwidth $W$, the UWB multiple access user capacity in bits/s can be obtained by

$$C^U_{M-PPM}(\gamma_I) = \frac{C_{M-PPM}(\gamma_I)}{T_s} \quad \text{[bits/s]}, \quad (6.22)$$

where $T_s$ is determined by bandwidth $W$ and spreading ratio $\rho$ as in (5.14).

In generating the figures in this section, we focused on the effect of MAI and thus ignored the effect of thermal noise. Fig. 6.4 and Fig. 6.5 present the user capacity in bits/s of UWB as a function of the number of users for various number of modulation levels $M$. The bandwidth is assumed as low band with $W = 3.1 - 5.15$GHz. The curves were obtained by Monte Carlo runs of (6.21) with $\rho = 5$ and $\rho = 10$ in Fig. 6.4 and Fig. 6.5 respectively.

For a better understanding of the trade-offs among the variables governing the user capacity, it is of interest to develop a closed form expression for (6.21). This is possible for the special case of $M = 2$. From (5.11), the user capacity in the presence

of MAI for binary PPM is given by

$$C(\gamma_I) = \frac{1}{2\sqrt{\pi}} \int_{-\infty}^{+\infty} \exp\left(-\frac{(x-\sqrt{\gamma_I})^2}{4}\right) \log_2\left(\frac{2}{1+\exp\left(-\sqrt{\gamma_I}x\right)}\right) dx. \qquad (6.23)$$

This expression is similar in form to [29, eq. (21)]. The expression in the reference was developed for direct sequence CDMA. Due to the similarity between the two expressions, other results from the reference can be of use. Using steps similar to [29, eq. (21)], it can be shown that a lower bound to the user capacity in the MAI regimen (6.23), is given by

$$C(\gamma_I) > 1 - \frac{\sqrt{2}\pi^2(\log_2 e)}{\pi^2-8}\left(\exp\left(-\frac{\pi^2-8}{4\pi^2}\gamma_I\right)\operatorname{erfc}\left(\frac{2\sqrt{\gamma_I}}{\pi}\right) - \frac{2\sqrt{2}}{\pi}\operatorname{erfc}\left(\frac{\sqrt{\gamma_I}}{2}\right)\right). \qquad (6.24)$$

A lower bound is of interest as it indicates the worst case of user capacity in the presence of MAI.

In Fig. 6.6, the lower bound (6.24) is plotted as a function of symbol SNR $\gamma_I$ along with the exact binary PPM capacity per (6.23). The capacity generated by Monte Carlo runs of (6.21) is also plotted for the comparison. It can be observed that the lower bound given in (6.24) is very close to the actual capacity, particularly for SNR values of interest $\gamma_I \geq 5$ dB.

The model for multi-user UWB assumes that each user contributes a fraction of the traffic in the channel. The aggregate capacity in the channel is obtained by summing all the user capacities,

$$\mathcal{C} = N_u C. \qquad (6.25)$$

Figure 6.7 presents the aggregate capacity in bits/s for binary PPM UWB with a bandwidth $W = 3.1 - 5.15$ GHz. The aggregate capacity is evaluated as a function of number of users for spreading ratios $\rho = 10$. The curves were generated using (6.23) and (6.25). From the figure it can be observed that when the number of the users is

increased without bound, the aggregate capacity converges to a constant value. The asymptotic capacities for $N_u \to \infty$ are also shown in the figure.

The upper bound on the multi-user aggregate capacity can be also proved theoretically. In the appendix it is shown that the individual user capacity for $\gamma_I \to 0$ is upper bound by

$$C(\gamma_I) < (\log_2 e)\frac{\gamma_I}{4}. \tag{6.26}$$

From (6.20) and (6.26), the aggregate capacity defined in (6.25) has an upper bound for small SNR $\gamma_I$

$$\mathcal{C} < (\log_2 e)\frac{3N_u\rho}{4(N_u-1)+12\rho/\gamma_0}. \tag{6.27}$$

When the number of users increases without bound, the aggregate capacity converges to

$$\lim_{N_u\to\infty} \mathcal{C} < (\log_2 e)\frac{3\rho}{4}. \tag{6.28}$$

Not surprisingly, this upper bound is proportional to the spreading ratio $\rho$.

## 6.3 Chapter Summary

In this chapter, the channel capacity of M-ary PPM UWB communications was computed over multiple-access channels. Under the assumptions, the multiple-access noise component at the receiver is modeled Gaussian. The SNR expressions is developed for UWB utilizing rectangular pulses. An expression for the UWB capacity for multiple-access channel is developed as a function of the number of users. A closed form expression was developed for the channel capacity for binary PPM. Using this expression, a lower bound was found for the user channel capacity. An upper bound was found for the aggregate capacity of all users. This upper bound is proportional to the spreading ratio $\rho$.

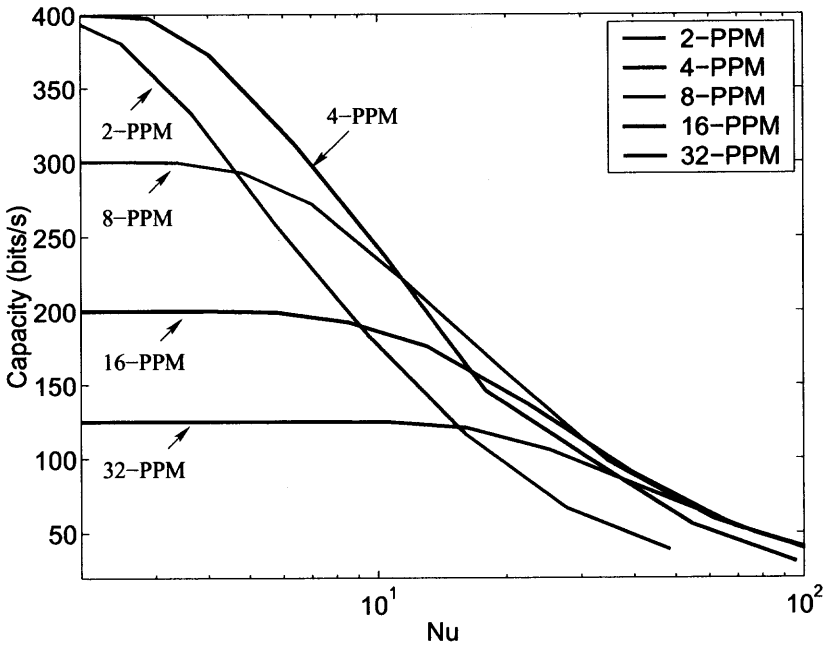


**Figure 6.4** User capacity of UWB multiple-access systems as a function of number of users $N_u$ for $\rho = 5$.

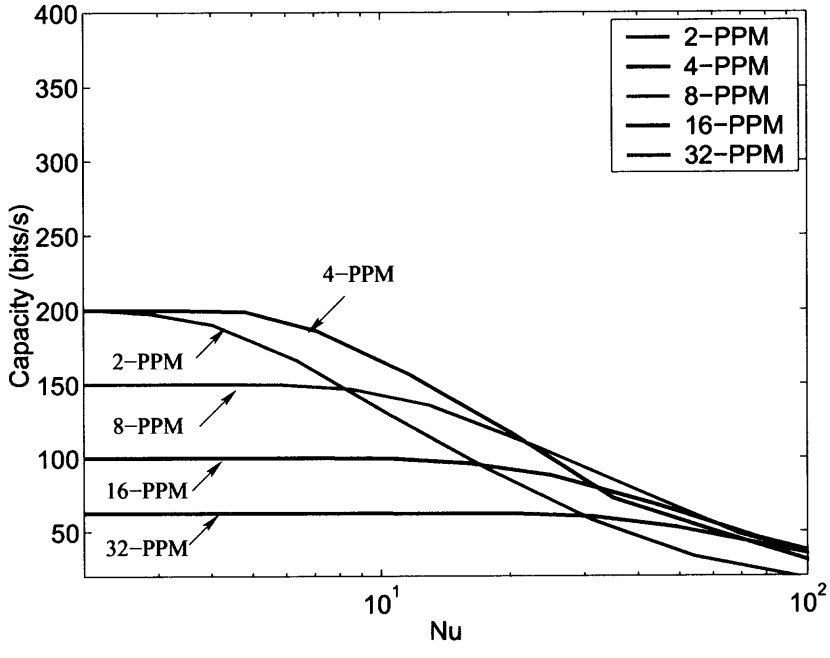


**Figure 6.5** User capacity for multi-user UWB as a function of number of users $N_u$ for $\rho = 10$.

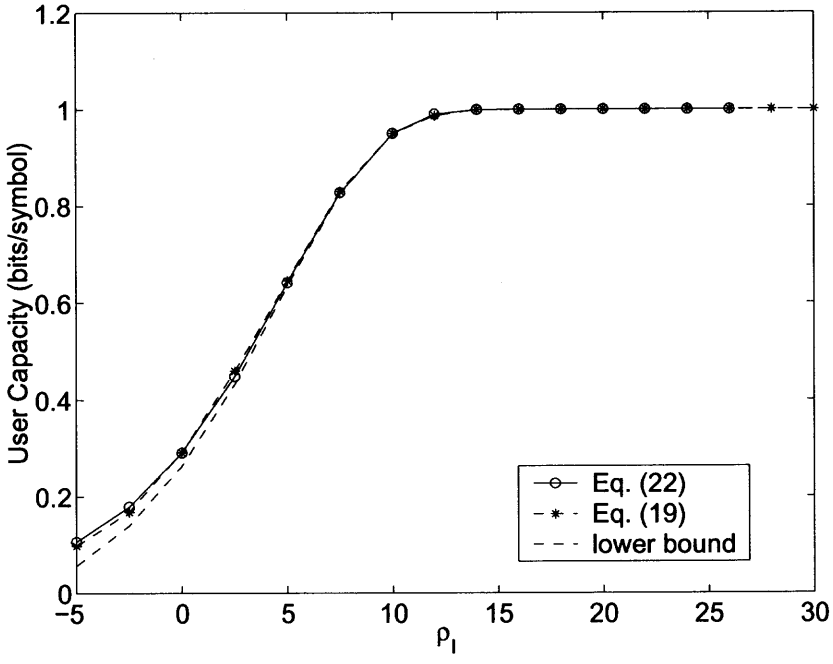


**Figure 6.6** User capacity of 2-PPM UWB system for spreading ratio $\rho = 100$.

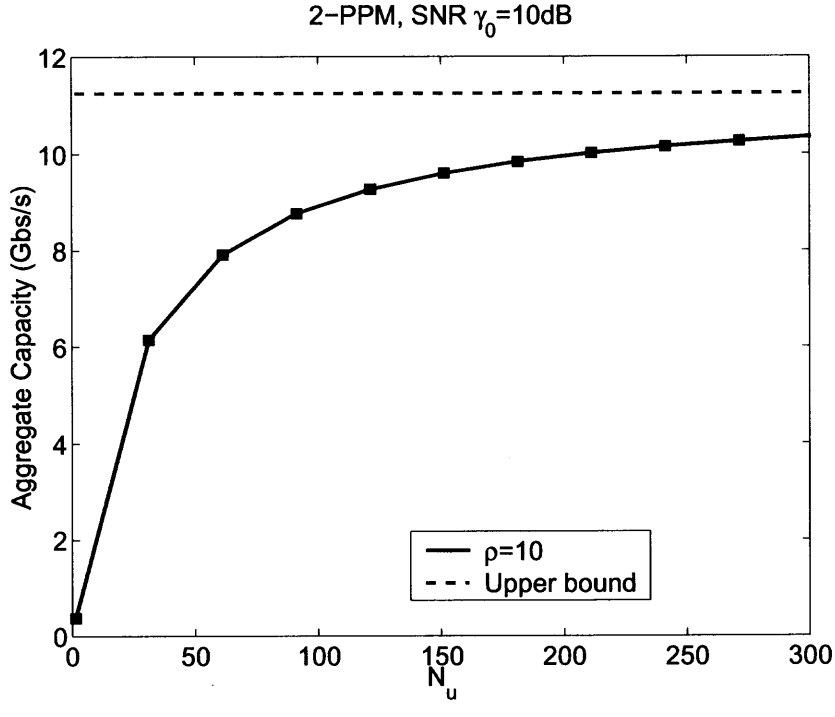


**Figure 6.7** Aggregate capacity of 2-PPM UWB systems as a function of number of users $N_u$ for $\gamma_0 = 10$ dB.

# CHAPTER 7

## SUMMARY OF DISSERTATION

The increased depletion of the frequency spectrum due to soaring wireless applications calls for the development of new efficient wireless technologies [30]. The existing paradigm of portions of the spectrum allocated to specific applications that ties up significant portions of the spectrum, even when the traffic is light, is not efficient. The UWB radio concept is very attractive as it promises to open large amounts of spectrum to a variety of users and at the same time it claims little interference between users. Not being subject to cochannel interference problems will lead to much simpler spectrum management schemes, maybe as far as no spectrum management required. Carrier-less signals will lead to simpler radios.

In addition, the increased interest in UWB communications is motivated by the assessment that this technology can provide reliable high data rate communications. Very low power spectral densities and high processing gain will enable overlay and ensure only minimal mutual interference between UWB and other applications. The ultra-wide bandwidth makes such communications robust with respect to multipath fading [24, 31, 32]. High ratios between the signal and information bandwidth (processing gain) makes this technology attractive to multiple access applications.

The original contribution of this research are:

- Assess the jam resistance of UWB using binary PPM.
- Compare the jam resistance capability between UWB and DS-SS under certain conditions.
- Investigate UWB link budget under FCC Part 15 Rules.

- Evaluate the information theoretic capacity of single-user M-ary modulated UWB wireless communications over AWGN and multipath channels.
- Calculate the user capacity and aggregate capacity for multiple-access UWB system using binary PPM.

# APPENDIX A

## UPPER BOUND ON CAPACITY OF BINARY PPM WITH MAI

In this appendix, we prove the upper bound (6.26) on the individual user capacity of binary PPM with MAI.

The exponential function can be expressed as a power series

$$\exp\left(-\sqrt{\gamma_I}x\right) = 1 + \sum_{n=1}^{+\infty} \frac{\left(-\sqrt{\gamma_I}x\right)^n}{n!}. \tag{A.1}$$

Using (A.1) in (5.11), the logarithm term is expanded in a power series

$$\begin{aligned}
&\log_2\left(\frac{2}{1+\exp\left(-\sqrt{\gamma_I}x\right)}\right) \\
&\quad = \left(-\log_2 e\right)\ln\left(1+\frac{\sum_{n=1}^{+\infty}\frac{\left(-\sqrt{\gamma_I}x\right)^n}{n!}}{2}\right) \\
&\quad = \left(\log_2 e\right)\sum_{m=1}^{+\infty}(-1)^m\frac{\left(\frac{1}{2}\sum_{n=1}^{+\infty}\frac{\left(-\sqrt{\gamma_I}x\right)^n}{n!}\right)^m}{m} \\
&\quad = \left(\log_2 e\right)\left(\frac{\sqrt{\gamma_I}x}{2}-\frac{\gamma_I x^2}{8}+\frac{\gamma_I^2 x^4}{192}-o\left[\gamma_I^3\right]\right),
\end{aligned} \tag{A.2}$$

where, by definition, if $f(\gamma) = o[\gamma^3]$, then $f(\gamma)/\gamma^3 \to 0$ as $\gamma \to 0$. It follows that for $\gamma$ sufficiently small, we have the upper bound

$$\log_2\left(\frac{2}{1+\exp\left(-\sqrt{\gamma_I}x\right)}\right) < \left(\log_2 e\right)\left(\frac{\sqrt{\gamma_I}x}{2}-\frac{\gamma_I x^2}{8}\right), \tag{A.3}$$

Substituting (A.3) into (5.11), we obtain the upper bound on the multi-user capacity

$$\begin{aligned}
C(\gamma_I) &< \frac{1}{2\sqrt{\pi}}\int_{-\infty}^{+\infty}\exp\left(-\frac{\left(x-\sqrt{\gamma_I}\right)^2}{4}\right)\left(\log_2 e\right) \\
&\quad \cdot\left(\frac{\sqrt{\gamma_I}x}{2}-\frac{\gamma_I x^2}{8}\right)dx \\
&= \left(\log_2 e\right)\left(\frac{\gamma_I}{4}-\frac{\gamma_I^2}{8}\right) \\
&< \left(\log_2 e\right)\frac{\gamma_I}{4}.
\end{aligned} \tag{A.4}$$

# APPENDIX B

## SUFFICIENT CONDITION FOR NO ISI

Define $\xi = (b_j - b_i)T_{PPM} - (n-m)T_f + \theta_l$. Note that $\alpha_{gp}(\tau) = 0$ when $\tau < -T_p$ or $\tau > T_g$. So, we have the sufficient condition for no ISI as following:

$$(b_j - b_i)T_{PPM} - (n-m)T_f + \theta_l < -T_p \tag{B.1}$$

$$\text{or} \qquad \Longrightarrow \quad \text{no ISI.}$$

$$(b_j - b_i)T_{PPM} - (n-m)T_f + \theta_l > T_g \tag{B.2}$$

Since $T_{PPM}$ is given as $T_{PPM} = T_f/M$, then $(b_j - b_i)T_{PPM} = \frac{j-i}{M}T_f$. In addition, because $0 < \theta_1 < T_m$, and $T_g = T_p + T_m$, the above condition can be written as following:

$$\left|\left(\frac{j-i}{M} - (n-m)\right)T_f + \left(\theta_l - \frac{T_m}{2}\right)\right| > T_p + \frac{T_m}{2} \quad \Longrightarrow \quad \text{no ISI.} \tag{B.3}$$

Using the inequality $|a+b| > |a| - |b|$, we can get two inequality,

$$\left|\left(\frac{j-i}{M} - (n-m)\right)T_f + \left(\theta_l - \frac{T_m}{2}\right)\right| > \left|\left(\frac{j-i}{M} - (n-m)\right)T_f\right| - \left|\theta_l - \frac{T_m}{2}\right|, \tag{B.4}$$

or

$$\left|\left(\frac{j-i}{M} - (n-m)\right)T_f + \left(\theta_l - \frac{T_m}{2}\right)\right| > \left|\theta_l - \frac{T_m}{2}\right| - \left|\left(\frac{j-i}{M} - (n-m)\right)T_f\right|. \tag{B.5}$$

Then we have the no ISI condition is:

$$\left|\left(\frac{j-i}{M} - (n-m)\right)\right|T_f - \left|\left(\theta_l - \frac{T_m}{2}\right)\right| > T_p + \frac{T_m}{2} \tag{B.6}$$

$$\text{or} \qquad \Longrightarrow \quad \text{no ISI.}$$

$$\left|\left(\theta_l - \frac{T_m}{2}\right)\right| - \left|\left(\frac{j-i}{M} - (n-m)\right)\right| T_f > T_p + \frac{T_m}{2} \tag{B.7}$$

Since $n = 1, .., N_p, m = 1, .., N_p$, and $n \neq m$, $i = 1, .., M, j = 1, ..., M$, we have

$$\min\left(\left|\frac{j-i}{M} - (n-m)\right|\right) = \frac{1}{M}. \tag{B.8}$$

In addition, because $\left|\theta_l - \frac{T_M}{2}\right| < \frac{T_M}{2}$, there is no solution for (B.7). We solve (B.7) and finally get condition for no ISI as following:

$$T_f > M(T_m + T_p) \quad \Longrightarrow \quad \text{no ISI for PPM.} \tag{B.9}$$

For the bi-phase and on-off keying modulation, $\xi$ is given as $\xi = (n-m)T_f + \theta_l$. Thus the condition of no ISI in (B.7) and (B.7) can be modified to bi-phase and on-off keying modulation as

$$|((n-m))|\, T_f - \left|\left(\theta_l - \frac{T_m}{2}\right)\right| > T_p + \frac{T_m}{2} \tag{B.10}$$

$$\text{or} \qquad \Longrightarrow \quad \text{no ISI.}$$

$$\left|\left(\theta_l - \frac{T_m}{2}\right)\right| - |((n-m))|\, T_f > T_p + \frac{T_m}{2} \tag{B.11}$$

and the condition can finally obtained

$$T_f > T_m + T_p \quad \Longrightarrow \quad \text{no ISI for bi-pahse and on-off keying.} \tag{B.12}$$

The condition for no SI can be obtained when $\xi$ is defined as $\xi = (b_j - b_i)T_{PPM} + \theta_l$ when $i \neq j$. Obviously SI only occur for PPM system, it never happen in the system utilizing bi-phase and on-off keying. After similar derivation as we did above, we have

$$\left|\frac{j-i}{M}\right| T_f - \left|\left(\theta_l - \frac{T_m}{2}\right)\right| > T_p + \frac{T_m}{2} \tag{B.13}$$

$$\text{or} \qquad \Longrightarrow \quad \text{no SI.}$$

$$\left|\left(\theta_l - \frac{T_m}{2}\right)\right| - \left|\frac{j-i}{M}\right| T_f > T_p + \frac{T_m}{2} \tag{B.14}$$

Since $\min\left(\left|\frac{j-i}{M}\right|\right) = 1/M$ for $i \neq j$, the condition of no SI is identical to the condition of no ISI for PPM system, e.g.,

$$T_f > M(T_m + T_p) \implies \text{no SI for PPM.} \tag{B.15}$$

## REFERENCES


[1] D. Leeper, "A long-term view of short-range wireless," *IEEE Computer Magzine*, vol. 34, June. 2001.

[2] Federal Communications Commission, "First report and order," *Docket No. 98-153*, pp. 1–118, Feb. 2002.

[3] M. Win, "Spectral density of random time-hopping spread-spectrum UWB signals with uniform timing jitter," *1999 Military Communications Conference (MILCOM '99)*, vol. 2, pp. 1196–1200, 1999.

[4] R. Scholtz, "Multiple access with time-hopping impulse modulation," *1993 Military Communications Conference (MILCOM '93)*, vol. 3, Oct. 1993.

[5] J. Massey, "Information theory aspects of spread-spectrum communications," *1994 IEEE International Symposium on Spread Spectrum Techniques and Applications (ISSSTA '94)*, pp. 17–21, 1994.

[6] P. Enge, K. Gromov, and J. Jung, "A cooperative program to assess interference from ultra wide band technologies to global positioning system," *1999 International UWB Conference*, Sep. 1999.

[7] G. Hurt, "Unlicensed radio devices: A study of aggregate interference," *1999 International UWB Conference*, Sep. 1999.

[8] L. Zhao and A. Haimovich, "Interference suppression in ultra-wideband communications," *35th Annual Conference on Information Sciences and Systems (CISS '01)*, pp. 759–763, Mar. 21-23 2001. Baltimore, Maryland.

[9] L. Zhao and A. Haimovich, "Performance of ultra-wideband communications in the presence of interference," *2001 IEEE International Conference on Communications (ICC '01)*, pp. 2948–2952, June. 11-15 2001. Helsinki, Finland.

[10] S. Dolinar, D. Divsalar, J. Hamkins, and F. Pollara, "Capacity of pulse-position mmodulation (PPM) on Gaussian and Webb channels," *JPL TMO Progress Report 42-142*, 2000.

[11] S. MacMullan and O.Collins, "The capacity of orthogonal codes on the Gaussian channel," *IEEE Transactions on Information Theory*, vol. 44, pp. 1217–1232, May 1998.

[12] T. Barrett, "History of ultra wide band (UWB) radar and communications: Pioneers and innovators," *Progress In Electromagnetics Symposium 2000*, July 2000.

[13] J. Conroy, J. LoCicero, and D. Ucci, "Communication techniques using monopulse waveforms," *1999 Military Communications Conference (MILCOM '99)*, vol. 2, pp. 1191–1185, 1999.

[14] Communication Research Lab (CRL) and XtremeSpectrum, "Merger No.2 proposal DS-UWB," IEEE 802.15-03/334r3.

[15] D. Cassioli, M. Win, and A. Molisch, "The ultra-wide bandwidth indoor channel: from statistical model to simulations," *IEEE Journal on Selected Areas on Communications*, vol. 20, pp. 1247–1257, Aug. 2002.

[16] Intel Corp., "Uwb channel modeling contribution," IEEE P802.15-02/02 790r0-SG3a.

[17] IEEE, "Channel modeling sub-committee final report," IEEE P802.15-02/02 490r0-SG3a.

[18] G. Weeks, J. Townsend, and J. Freebersyser, "Quantifying the covertness of pulse radio," *1999 International UWB Conference*, Sep. 1999.

[19] J. Proakis and M. Salehi, *Communication Systems Engineering.* Prentice Hall, 1994.

[20] L. Zhao and A. Haimovich, "Performance of ultra-wideband communications in the presence of interference," *IEEE Journal on Selected Area in Communications*, vol. 20, pp. 1684–1691, Dec. 2002.

[21] K. Kamakura, T. Ohtsuki, H. Uehara, Y. Gamachi and I. Sasase, "Optical spread time CDMA communications system with PPM signaling," *1998 IEEE International Symposium on Information Theory (ISIT '98)*, vol. 1, p. 258, 1998.

[22] M. Win, G. Chrisikos, and N. Sollenberger, "Performance of rake reception in dense multipath channel: Implications of spreading bandwidth and selection diversity order," *IEEE Journal on Selected Areas in Communications*, vol. 18, pp. 1516–1525, Aug. 2000.

[23] L. Zhao and A. Haimovich, "Multi-user capacity of M-ary PPM ultra-wideband communications," *2002 IEEE Conference on Ultra Wideband Systems and Technologies (UWBST '02)*, pp. 175–180, May. 21-24 2002. Baltimore, Maryland.

[24] M. Win, *Ultra-wide Bandwidth Spread-Spectrum Techniques for Wireless Multiple-Access Communications.* PhD thesis, Electrical Engineering, University of Southern California, Los Angeles, CA., Jan. 1998.

[25] M. Win and R. Scholtz, "Ultra-wide bandwidth time-hopping spread-spectrum impulse radio for wireless multiple-access communications," *IEEE Transactions on Communications*, vol. 48, pp. 679–691, Apr. 2000.

[26] L. Zhao and A. Haimovich, "Capacity of M-ary PPM ultra-wideband communications over AWGN channels," *2001 fall IEEE Vehicular Technology Conference (VTC '2001 fall)*, pp. 1191–1195, Oct. 7-11 2001.

[27] F. Ramirez-Mireles, "Performance of ultra wideband SSMA using time-hopping and M-ary PPM," *IEEE Journal on Selected Areas in Communications*, vol. 19, pp. 1186–1196, June. 2001.

[28] F. Ramirez-Mireles and R. Scholtz, "Multiple access performance of ultra-wideband spread spectrum impulse radio using block waveform modulation," *1998 IEEE International Conference on Communications (ICC '98)*, Jun. 1998.

[29] M. Alencar and I. Blake, "The capacity for a discrete-state code division multiple-access channel," *IEEE Journal on Selected Areas in Communications*, vol. 12, pp. 925–937, June. 1994.

[30] T. Shepard, "Getting the most value out of the radio spectrum," *1999 International UWB Conference*, Sep. 1999.

[31] M. Win and R. Scholtz, "Impulse radio: How it works," *IEEE Communications Letters*, Feb. 1998.

[32] R. Cramer, M. Win, and R. Scholt, "Evaluation of the multipath characteristics of the impulse radio channel," *1998 International Symposium on Personal, Indoor and Mobile Radio Communications (PIMRC' 98)*, 1998.